

การปรับปรุงสภาพให้ออกซิเจนซึมผ่านได้ของเมมเบรนเพอรอฟสไกต์ฐานแบเรียมหรือแลนทานัม  
โดยการเคลือบผิวด้วยตัวเร่งปฏิกิริยา

นายสุนทร สุวอเขียว

วิทยานิพนธ์นี้เป็นส่วนหนึ่งของการศึกษาตามหลักสูตรปริญญาวิทยาศาสตรมหาบัณฑิต  
สาขาวิชาเคมี ภาควิชาเคมี  
คณะวิทยาศาสตร์ จุฬาลงกรณ์มหาวิทยาลัย  
ปีการศึกษา 2553  
ลิขสิทธิ์ของจุฬาลงกรณ์มหาวิทยาลัย

IMPROVING THE OXYGEN PERMEABILITY OF BARIUM OR LANTHANUM-  
BASED PEROVSKITE MEMBRANES BY SURFACE-COATING WITH  
CATALYSTS

Mr. Soontorn Suvokhiaw

A Thesis Submitted in Partial Fulfillment of the Requirements  
for the Degree of Master of Science Program in Chemistry

Department of Chemistry

Faculty of Science

Chulalongkorn University

Academic Year 20010

Copyright of Chulalongkorn University

Thesis Title           IMPROVING THE OXYGEN PERMEABILITY OF  
                                  BARIUM OR LANTHANUM-BASED PEROVSKITE  
                                  MEMBRANES BY SURFACE-COATING WITH  
                                  CATALYSTS

By                         Mr. Soontorn Suvokhiaw

Field of Study         Chemistry

Thesis Advisor        Nipaka Sukpirom, Ph.D.

Thesis Co-advisor    Assistant Professor Jinda Yeyongchaiwat, Ph.D.

---

Accepted by the Faculty of Science, Chulalongkorn University in Partial  
Fulfillment of the Requirements for the Master's Degree

.....Dean of the Faculty of Science  
(Professor Supot Hannongbua, Dr. rer. nat)

#### THESIS COMMITTEE

.....Chairman  
(Assistant Professor Soamwadee Chaianansutcharit, Ph.D.)

.....Thesis Advisor  
(Nipaka Sukpirom, Ph.D.)

.....Thesis Co-advisor  
(Assistant Professor Jinda Yeyongchaiwat, Ph.D.)

.....Examiner  
(Assistant Professor Boosayarat Tomapatanaget, Ph.D.)

.....External Examiner  
(Sumittra Charojrochkul, Ph.D.)

สุนทร สุวอเขียว : การปรับปรุงสภาพให้ออกซิเจนซึมผ่านได้ของเมมเบรนเพอโรฟสไกต์  
ฐานแบเรียมหรือแลนทานัมโดยการเคลือบผิวด้วยตัวเร่งปฏิกิริยา (IMPROVING THE  
OXYGEN PERMEABILITY OF BARIUM OR LANTHANUM-BASED  
PEROVSKITE MEMBRANES BY SURFACE-COATING WITH  
CATALYSTS) อ. ที่ปริกษาวิทยานิพนธ์หลัก: อ.ดร. นิปกา สุขภิรมย์, อ. ที่ปริกษา  
วิทยานิพนธ์ร่วม: ผู้ช่วยศาสตราจารย์ ดร.จินดา ยืนยงชัยวัฒน์, 70 หน้า.

ศึกษาผลของการเคลือบตัวเร่งปฏิกิริยา  $\text{SrCoFeO}_x$  (SCF),  $\text{La}_{0.1}\text{Sr}_{0.9}\text{Co}_{0.9}\text{Fe}_{0.1}\text{O}_3$  (LSCF) และ  $\text{SrCo}_{0.4}\text{Fe}_{0.5}\text{Ni}_{0.1}\text{O}_3$  (SCFN) ซึ่งเตรียมโดยวิธี Modified citrate ลงบนผิวของเมมเบรน  $\text{Ba}_{0.5}\text{Sr}_{0.5}\text{Co}_{0.8}\text{Fe}_{0.2}\text{O}_3$  (BSCF) และ  $\text{BaCo}_{0.7}\text{Fe}_{0.2}\text{Nb}_{0.1}\text{O}_3$  (BCFN) ซึ่งเตรียมโดยวิธี Solid state ต่อความสามารถในการซึมผ่านของออกซิเจนของเมมเบรน BSCF และ BCFN แต่เนื่องจากความหนาแน่นสัมพัทธ์ของเมมเบรน BCFN มีค่า 79.28% ซึ่งเป็นค่าน้อยกว่าค่าที่เหมาะสม (90%) สำหรับใช้เป็นเมมเบรนเลือกผ่านแก๊ส ดังนั้นเฉพาะเมมเบรน BSCF เท่านั้นที่สามารถนำไปศึกษาต่อได้ ขั้นแรกเคลือบผิวของเมมเบรน BSCF ด้วยตัวเร่งปฏิกิริยาที่เตรียมได้ทั้งการเคลือบแบบด้านเดียวและสองด้านแล้วหาความสามารถในการซึมผ่านของออกซิเจนที่อุณหภูมิ 700 – 1000 องศาเซลเซียส พบว่าเมมเบรนที่เคลือบผิวด้วยตัวเร่งปฏิกิริยามักมีอัตราการซึมผ่านของออกซิเจนมากกว่าเมมเบรนที่ไม่ได้เคลือบผิวด้วยตัวเร่งปฏิกิริยา และเมื่อเปรียบเทียบผลการเคลือบตัวเร่งปฏิกิริยาบนผิวของเมมเบรนด้านที่มี Oxygen partial pressure สูง (ด้านอากาศ) เพียงด้านเดียว พบว่า SCF สามารถเพิ่มอัตราซึมผ่านออกซิเจนให้แก่เมมเบรน BSCF ได้มากกว่า LSCF และ SCFN ส่วนผลการเคลือบตัวเร่งปฏิกิริยาบนผิวของเมมเบรนด้านที่มี Oxygen partial pressure ต่ำ (ด้านฮีเลียม) เพียงด้านเดียว พบว่า SCFN สามารถเพิ่มอัตราซึมผ่านออกซิเจนให้แก่เมมเบรน BSCF ได้มากกว่า LSCF และ SCF จากนั้นจึงเลือกตัวเร่งที่ดีที่สุดในแต่ละด้านมาเคลือบบนเมมเบรนคือ SCF สำหรับเคลือบด้านอากาศและ SCFN สำหรับเคลือบด้านฮีเลียม และพบว่าสามารถเพิ่มอัตราซึมผ่านออกซิเจนให้แก่เมมเบรน BSCF ได้มากกว่าการเคลือบแค่เพียงด้านเดียวและมีความเสถียรต่อการซึมผ่านออกซิเจนที่อุณหภูมิ 850 องศาเซลเซียสไม่ต่ำกว่า 100 ชั่วโมง สุดท้ายได้ศึกษาความเข้ากันได้ทางเคมีของเมมเบรนและตัวเร่งปฏิกิริยาโดยทดสอบเผาเป็นเวลา 10 ชั่วโมง พบว่าอุณหภูมิสูงสุดที่เมมเบรน BSCF สามารถเข้ากันได้ดีกับ SCF และ SCFN คือ 850 องศาเซลเซียส และ LSCF คือ 900 องศาเซลเซียส

สาขาวิชา ..... เคมี ..... ลายมือชื่อนิสิต .....

ปีการศึกษา ..... 2553 ..... ลายมือชื่อ อ. ที่ปริกษาวิทยานิพนธ์หลัก .....

ลายมือชื่อ อ. ที่ปริกษาวิทยานิพนธ์ร่วม .....

# # 5172508923: MAJOR CHEMISTRY

KEYWORDS: OXYGEN PERMEABILITY / OXYGEN PERMEATION / SURFACE MODIFICATION / SURFACE COATING / BARIUM OR LANTHANUM-BASED PEROVSKITE

SOONTORN SUVOKHIAW: IMPROVING THE OXYGEN PERMEABILITY OF BARIUM OR LANTHANUM-BASED PEROVSKITE MEMBRANES BY SURFACE-COATING WITH CATALYSTS. ADVISOR: NIPAKA SUKPIROM, Ph.D., CO-ADVISOR: ASSISTANT PROFESSOR JINDA YEYONGCHAIWAT, Ph.D., 70 pp.

The effect of  $\text{SrCoFeO}_x$  (SCF),  $\text{La}_{0.1}\text{Sr}_{0.9}\text{Co}_{0.9}\text{Fe}_{0.1}\text{O}_3$  (LSCF) and  $\text{SrCo}_{0.4}\text{Fe}_{0.5}\text{Ni}_{0.1}\text{O}_3$  (SCFN) thin layers, prepared by modified citrate method, coating on oxygen permeation flux through dense  $\text{Ba}_{0.5}\text{Sr}_{0.5}\text{Co}_{0.8}\text{Fe}_{0.2}\text{O}_3$  (BSCF) membranes and  $\text{BaCo}_{0.7}\text{Fe}_{0.2}\text{Nb}_{0.1}\text{O}_3$  (BCFN) membranes, synthesized via solid state method, was investigated. Unfortunately, the relative density of prepared BCFN membrane (79.28%) was quite lower than the required 90% for gas permeation membrane; therefore, only BSCF membrane was further studied. The catalyst powders were coated on one or both surfaces of dense BSCF membranes. The oxygen permeation flux of membranes was measured in the temperature range of 700-1000°C. The results show that the oxygen permeation fluxes of most coated membranes were higher than the flux of uncoated BSCF membrane. Comparing the effect of single-coating on air side, coating of SCF showed higher flux than coating with LSCF and SCFN. On the other hand, comparing the effect on He side, coating with SCFN gave higher flux than LSCF and SCF. Furthermore, double coating with SCF on air side and with SCFN on He side increased the flux of a single-coating and has good oxygen permeation stability at 850°C for at least 100h. The chemical compatibility of membrane and catalysts was tested by firing at high temperature for 10 h. BSCF membrane has good compatibility with SCF and SCFN at 850°C and with LSCF at 900°C.

Field of Study : ..... Chemistry ..... Student's Signature .....

Academic Year : ..... 2010 ..... Advisor's Signature .....

Co-advisor's Signature .....

## ACKNOWLEDGEMENTS

The author deeply appreciates his family for their love, support and encouragement during the period of his study.

The author wishes to express greatest gratitude to his advisor, Dr. Nipaka Sukpirom, for her valuable advice, kind assistance, and encouragement throughout the course of this research. Gratefully thanks to Assistant Professor Dr. Jinda Yeyongchaiwat, for her good advice, kind assistance and the support on equipments. In addition, the author would like to thank to Assistant Professor Soamwadee Chaianansutcharit, Assistant Professor Boosayarat Tomapatanaget and Dr. Sumittra Charojrochkul for serving as the chairman and examiner of his thesis committee, respectively, for their valuable suggestions and comments. The author would like to thank to Assistant Professor Dr. Soamwadee Chaianansutcharit for the support on the equipments and kind assistance.

The successful of this thesis fulfill by some part of research which is done by Mister Karuna Nontawisaroot. So the author gratefully thanks him.

The author would like to thank the Materials for Energy Research Unit, National Metal and Materials Technology Center (MTEC) and Department of Chemistry, Faculty of Science and technology, Bansomdejchaopraya Rajabhat University for the support on the equipments.

Appreciation is extended to Materials Chemistry and Catalysis Research Unit (MATCAT) for provision of experimental facilities. Acknowledgement is also extended to Department of Chemistry, Faculty of Science, Chulalongkorn University and Center for Petroleum, Petrochemicals, and Advanced Materials for granting financial support to fulfill this study as well as Development and Promotion of Science and Technology (DPST).

This thesis cannot be completed without generous help of the staff members of the Materials Chemistry and Catalysis Research Unit (MATCAT). Special thank is forwarded to his best friends for their love, assistance and encouragement. Without them, the author would have never been able to achieve this goal.

## CONTENTS

	<b>Page</b>
<b>ABSTRACT IN THAI</b> .....	iv
<b>ABSTRACT IN ENGLISH</b> .....	v
<b>ACKNOWLEDGEMENTS</b> .....	vi
<b>CONTENTS</b> .....	vii
<b>LIST OF TABLES</b> .....	x
<b>LIST OF FIGURES</b> .....	xi
<b>LIST OF ABBREVIATIONS</b> .....	xiv
<b>CHAPTER I INTRODUCTION</b> .....	1
1.1 Background .....	1
1.2 Literature review of membrane materials .....	1
1.2.1 BSCF .....	2
1.2.2 BCFN .....	3
1.3 Literature review of catalyst materials .....	4
1.3.1 SCF.....	4
1.3.2 LSCF.....	4
1.3.3 SCFN.....	5
1.4 Literature review of surface modification .....	5
1.5 The objectives of this study .....	6
<b>CHAPTER II THEORY</b> .....	7
2.1 Oxygen separation from air using Ceramic membranes .....	7
2.2 Perovskite structure .....	8
2.3 Ceramic compounds preparation methods .....	9
2.4 Powder compacting by uniaxial pressing.....	10
2.5 Sintering .....	11
2.6 Phase characterization of materials .....	11
2.7 Oxygen transport .....	13
2.7.1 Bulk-diffusion limited.....	14

	<b>Page</b>
2.7.2 Surface-exchange limited.....	15
2.8 Oxygen permeation flux .....	16
<b>CHAPTER III EXPERIMENTAL</b> .....	<b>17</b>
3.1 Chemicals .....	17
3.2 Synthesis of materials .....	17
3.2.1 Preparation of $\text{Ba}_{0.5}\text{Sr}_{0.5}\text{Co}_{0.8}\text{Fe}_{0.2}\text{O}$ membrane.....	17
3.2.2 Preparation of $\text{BaCo}_{0.7}\text{Fe}_{0.2}\text{Nb}_{0.1}\text{O}_3$ membrane.....	18
3.2.3 Synthesis of $\text{La}_{0.1}\text{Sr}_{0.9}\text{Co}_{0.9}\text{Fe}_{0.1}\text{O}_3$ .....	18
3.2.4 Synthesis of $\text{SrCoFeO}_x$ .....	18
3.2.5 Synthesis of $\text{SrCo}_{0.4}\text{Fe}_{0.5}\text{Ni}_{0.1}\text{O}_3$ .....	19
3.3 Characterization of materials .....	19
3.6.1 Powder X-ray diffraction (XRD) .....	19
3.6.2 Electrochemical impedance spectroscopy (EIS) .....	19
3.4 Catalytic coating .....	20
3.4.1 Single-coating .....	20
3.4.2 Double-coating .....	20
3.5 Oxygen permeation .....	21
3.6 Stability of coating-membranes .....	21
3.6.1 Chemical compatibility of membranes and catalysts .....	21
3.6.2 Long-term oxygen permeation flux .....	22
<b>CHAPTER IV RESULTS AND DISCUSSION</b> .....	<b>23</b>
4.1 Synthesis and characterization .....	23
4.1.1 Crystal structure of membrane materials .....	23
4.1.2 Crystal structure of catalyst materials .....	25
4.2 Conductivity of membranes .....	27
4.3 Oxygen permeation .....	28
4.3.1 Oxygen permeation of BSCF membranes.....	28
4.3.1.1 Single-coating BSCF membrane .....	28
4.3.1.2 Double coating BSCF membrane .....	30



	<b>Page</b>
4.3.2 Oxygen permeation of BCFN membrane.....	32
4.4 Compatibility between membranes and catalysts .....	35
4.4.1 Compatibility between membranes and catalysts monitored by XRD .....	35
4.4.2 Compatibility between membranes and catalysts monitored by SEM/EDS .....	38
4.4.2.1 Surface of coated and uncoated membranes .....	38
4.4.2.2 Cross section of coated and uncoated membranes .....	43
4.5 Long-term stability .....	48
<b>CHAPTER V CONCLUSION AND SUGGESTION.....</b>	<b>49</b>
5.1 Conclusion.....	49
5.2 Suggestion.....	50
<b>REFERENCES.....</b>	<b>51</b>
<b>APPENDICES.....</b>	<b>56</b>
<b>VITAE.....</b>	<b>70</b>

## LIST OF TABLES

<b>Table</b>		<b>Page</b>
3.1	The detailed list of chemicals and reagents.....	17
3.2	List of the catalytic coating on membranes.....	20
4.1	Crystal structure, lattice parameters, density and relative density of BSCF, BCFN, LSCF, SCF and SCFN.....	25
4.2	Relative densities of BCFN membrane prepared from the powder calcined at various temperatures.....	34
4.3	Relative densities of BCFN membrane prepared at different pressure.....	34

## LIST OF FIGURES

<b>Figure</b>	<b>Page</b>	
2.1	Types of oxygen separation system; a) pure oxygen conducting membrane, and b) mixed ionic electronic (i) single phase conducting membrane and (ii) dual phase conducting membrane.....	7
2.2	Schematic representation of the oxygen transport through mixed conducting membrane .....	8
2.3	Simple drawing of perovskite structure ( $ABO_3$ ).....	9
2.4	Mechanism of sintering.....	11
2.5	Different sections involved in oxygen transport during oxygen permeation .....	13
2.6	Variation of regime from bulk-diffusion to surface-exchange reaction limited with decreasing membrane thickness.....	14
3.1	Schematic diagram of the membrane reactor setup for oxygen permeation study.....	21
4.1	XRD pattern of as-prepared BSCF. ....	23
4.2	XRD pattern of as-prepared BCFN .....	24
4.3	XRD pattern of as-prepared LSCF.....	26
4.4	XRD pattern of as-prepared SCFN.....	26
4.5	XRD pattern of as prepared SCF .....	27
4.6	Electrical conductivity of BSCF and BCFN at 400-850°C.....	28
4.7	Oxygen permeation fluxes of uncoated and coated BSCF membranes on a) the air side and b) the He side .....	29
4.8	Oxygen permeation fluxes of uncoated, single-coated and double-coated BSCF membranes by SCF on the air side and LSCF on the He side.....	31
4.9	Oxygen permeation fluxes of uncoated, single-coated and double-coated BSCF membranes by SCF on the air side and SCFN on the He side.....	31

<b>Figure</b>	<b>Page</b>
4.10 Oxygen permeation fluxes of uncoated and double-coated BSCF membranes.....	32
4.11 XRD patterns of BCFN membranes at various sintering temperatures.....	34
4.12 XRD patterns of the mixture of BSCF and LSCF powders firing from 800°C to 1000°C in the period of 10 h for each temperature.....	36
4.13 XRD patterns of the mixture of BSCF and SCFN powders firing from 800°C to 1000°C in the period of 10 h for each temperature.....	37
4.14 XRD patterns of the mixture of BSCF and SCF powders firing from 800°C to 1000°C in the period of 10 h for each temperature.....	38
4.15 SEM images of the surface of BSCF membrane before and after being tested for oxygen permeation; a) before, b) air side, c) He side and d) the EDS analysis of a) – c).....	40
4.16 SEM images of the surface of BSCF membrane coated by SCF before and after being tested for oxygen permeation; a) before, b) air side, c) He side and d) the EDS analysis of a) – c).....	41
4.17 SEM images of the surface of BSCF membrane coated by LSCF before and after being tested for oxygen permeation; a) before, b) air side, c) He side and d) the EDS analysis of a) – c).....	42
4.18 SEM images of the surface of BSCF membrane coated by SCFN before and after being tested for oxygen permeation; a) before, b) air side, c) He side and d) the EDS analysis of a) – c).....	43
4.19 SEM images of the cross section of BSCF membrane coated with SCF on the air side before and after being tested for oxygen permeation.....	45
4.20 SEM images of the cross section of BSCF membrane coated with SCF on the He side before and after being tested for oxygen permeation.....	45

<b>Figure</b>		<b>Page</b>
4.21	SEM images of the cross section of BSCF membrane coated with LSCF on the air side before and after being tested for oxygen permeation.....	46
4.22	SEM images of the cross section of BSCF membrane coated with LSCF on the He side before and after being tested for oxygen permeation.....	46
4.23	SEM images of the cross section of BSCF membrane coated with SCFN on the air side before and after being tested for oxygen permeation .....	47
4.24	SEM images of the cross section of BSCF membrane coated with SCFN on the He side before and after being tested for oxygen permeation.....	47
4.25	The long-term stability of BSCF membrane that was coated with SCF on the air side and SCFN on the He side at 850°C.....	48

## LIST OF ABBREVIATIONS

°C	Degree Celsius
min	Minute or minutes
mL	Mililite
Å	Angstrom unit
XRD	X-ray diffraction
SEM	Scanning electron microscopy
SEM-EDX	Scanning electron microscopy-energy dispersive X-ray fluorescence
EIS	Electrochemical Impedance Spectroscopy
h	Hour or hours
mol %	Percent by mole
wt %	Percent by weight
MIEC	Mixed Electronic and Ionic Conductors
ABO <sub>3</sub>	Perovskite structure
p(O <sub>2</sub> )	Partial pressure of oxygen
BSCF	Perovskite containing Ba, Sr, Co and Fe
BCFN	Perovskite containing Ba, Co, Fe and Nb
LSCF	Perovskite containing La, Sr, Co and Fe
SCF	Metals oxide containing Sr, Co and Fe
SCFN	Perovskite containing Sr, Co, Fe and Ni

# CHAPTER I

## INTRODUCTION

### 1.1 Background

Oxygen market becomes a big business in the future because the green energy technology requires oxygen gas as a feed such as electricity production, chemical process operation, fuel cell, steel industry, and a reactant for syngas reaction etc [1-3]. As an old technology, oxygen was produced by cryogenic distillation. The inlet air must be compressed and chilled until the temperature reaches  $-185^{\circ}\text{C}$ . Thereafter, the liquid must be distilled at the plant according to the boiling points of air components. This method gave the purity of oxygen about 95%. The cryogenic distillation method is not only expensive but also corrosive. Nowadays, dense mixed ionic-electronic conducting (MIEC) ceramic membrane is a candidate of new materials for oxygen separation membrane because it can separate 100% oxygen gas from air without the use of external electric loading and the membrane technology is considered as a low cost separation technology [4].

Some perovskite materials are mixed ionic-electronic conductor, due to the presence of oxygen vacancy sites in their structure. They are introduced as cathode materials for solid oxide fuel cell (SOFC), membranes for syngas production and membranes for oxygen separation. In this thesis, their oxygen permeation ability is of interest [4].

The oxygen transport through dense membrane involves two mechanisms; the oxide ion diffusion through bulk phase and oxygen surface-exchange on the surface of membrane. Therefore, in order to enhance the oxygen permeation flux, two approaches, decreasing the membrane thickness and surface modification by materials with high oxygen sorption/desorption rate were suggested [4].

### 1.2 Literature review of membrane materials

The materials used as membranes for oxygen separation must possess several important properties such as high oxygen permeation flux, structural stability at

operating temperatures and mixed ionic-electronic property. According to the literature reviews below, two materials were selected for this research.

### 1.2.1 BSCF

The oxygen permeable materials must have mixed ionic electronic property. Conductive Perovskites are widely known to have such property [5].

$\text{SrCo}_{0.8}\text{Fe}_{0.2}\text{O}_{3-\delta}$  was one of the first materials which was a candidate for an oxygen transport membrane because of its high oxygen permeation flux [6]. However, Qiu *et al.* [7] reported that  $\text{SrCo}_{0.8}\text{Fe}_{0.2}\text{O}_{3-\delta}$  has limited chemical and structural stability in reduced environments. Moreover Pei *et al.* [8] reported that  $\text{SrCo}_{0.8}\text{Fe}_{0.2}\text{O}_{3-\delta}$  transformed to a low oxygen-conductive brownmillerite in the low oxygen partial pressure environment at the temperature of 800°C. Shao *et al.* [9] reported that the partial substitution of strontium by barium in  $\text{SrCo}_{0.8}\text{Fe}_{0.2}\text{O}_3$  could stabilize the perovskite structure and result in a higher oxygen flux than  $\text{SrCo}_{0.8}\text{Fe}_{0.2}\text{O}_3$ . The  $\text{Ba}_{0.5}\text{Sr}_{0.5}\text{Co}_{0.8}\text{Fe}_{0.2}\text{O}_{3-\delta}$  membrane could operate stably as an oxygen generator at 850°C. Wang *et al.* [10] investigated the stability and oxygen permeation property of  $\text{Ba}_{0.5}\text{Sr}_{0.5}\text{Co}_{0.8}\text{Fe}_{0.2}\text{O}_{3-\delta}$  compared to those of  $\text{SrCo}_{0.8}\text{Fe}_{0.2}\text{O}_{3-\delta}$ . They reported that the phase stability increased with the partial substitution of strontium by barium. Moreover, the oxygen permeation was still kept at high level, such that, for  $\text{Ba}_{0.5}\text{Sr}_{0.5}\text{Co}_{0.8}\text{Fe}_{0.2}\text{O}_{3-\delta}$  with the thickness of 1.8 mm, the oxygen permeation flux reached about 1.4 ml/cm<sup>2</sup>min at 950°C. Wang *et al.* [11] investigated the in situ phase structures of  $\text{Ba}_{0.5}\text{Sr}_{0.5}\text{Co}_{0.8}\text{Fe}_{0.2}\text{O}_{3-\delta}$  at high temperatures and the influence of the sintering conditions on oxygen permeability of  $\text{Ba}_{0.5}\text{Sr}_{0.5}\text{Co}_{0.8}\text{Fe}_{0.2}\text{O}_{3-\delta}$ . The results showed that  $\text{Ba}_{0.5}\text{Sr}_{0.5}\text{Co}_{0.8}\text{Fe}_{0.2}\text{O}_{3-\delta}$  exhibited good phase reversibility and structural stability both in air and in pure argon. Moreover, the oxygen permeation flux of  $\text{Ba}_{0.5}\text{Sr}_{0.5}\text{Co}_{0.8}\text{Fe}_{0.2}\text{O}_{3-\delta}$  increased with increasing grain size. The thermal expansion coefficient of  $\text{Ba}_{0.5}\text{Sr}_{0.5}\text{Co}_{0.8}\text{Fe}_{0.2}\text{O}_{3-\delta}$  ( $11.5 \times 10^{-6} \text{ K}^{-1}$ ) was smaller than  $\text{SrCo}_{0.8}\text{Fe}_{0.2}\text{O}_{3-\delta}$  ( $17.9 \times 10^{-6} \text{ K}^{-1}$ ). McIntosh *et al.* [12] reported that  $\text{Ba}_{0.5}\text{Sr}_{0.5}\text{Co}_{0.8}\text{Fe}_{0.2}\text{O}_{3-\delta}$  had a higher oxygen vacancy concentration than  $\text{SrCo}_{0.8}\text{Fe}_{0.2}\text{O}_{3-\delta}$  which was the reason behind the higher oxygen permeation flux than  $\text{SrCo}_{0.8}\text{Fe}_{0.2}\text{O}_{3-\delta}$ . Liu *et al.* [13] reported that  $\text{Ba}_{0.5}\text{Sr}_{0.5}\text{Co}_{0.8}\text{Fe}_{0.2}\text{O}_{3-\delta}$  can be used as the cathode for IT-SOFC. Bo *et al.* [14] reported that at 850°C,  $\text{Ba}_{0.5}\text{Sr}_{0.5}\text{Co}_{0.8}\text{Fe}_{0.2}\text{O}_{3-\delta}$  had a lower area specific resistance (ASR) of  $\text{Ba}_{0.5}\text{Sr}_{0.5}\text{Co}_{0.8}\text{Fe}_{0.2}\text{O}_{3-\delta}/\text{Y}_2\text{O}_3$ -stabilized zirconia ( $0.077 \text{ } \Omega\text{cm}^2$ ) than the



commonly used materials  $\text{La}_{0.8}\text{Sr}_{0.2}\text{MnO}_{3-\delta}$  and exhibited much better performance of single cell of SCFC than  $\text{La}_{0.8}\text{Sr}_{0.2}\text{MnO}_{3-\delta}$ . Zeng *et al.* [15] reported that  $\text{Ba}_{0.5}\text{Sr}_{0.5}\text{Co}_{0.8}\text{Fe}_{0.2}\text{O}_{3-\delta}$  was promising as materials for oxygen separation membrane. Although  $\text{Ba}_{0.5}\text{Sr}_{0.5}\text{Co}_{0.8}\text{Fe}_{0.2}\text{O}_{3-\delta}$  had a smaller electronic conductivity than  $\text{SrCo}_{0.8}\text{Fe}_{0.2}\text{O}_{3-\delta}$  but the oxygen permeation and ionic conductivity were higher. Moreover, they reported that the permeation rate of  $\text{Ba}_{0.5}\text{Sr}_{0.5}\text{Co}_{0.8}\text{Fe}_{0.2}\text{O}_{3-\delta}$  with the thickness about 1.5 mm was controlled by the oxygen surface exchange at the low partial pressure side. Baumann *et al.* [16] reported that, for  $\text{Ba}_{0.5}\text{Sr}_{0.5}\text{Co}_{0.8}\text{Fe}_{0.2}\text{O}_{3-\delta}$  membrane with thickness of 1 mm, neither the porosity nor the grain size influenced the oxygen permeation rate significantly.

### 1.2.2 BCFN

Zhang *et al.* [17] reported the total conductivity, oxygen permeability and stability of  $\text{BaCo}_{0.7}\text{Fe}_{0.2}\text{Nb}_{0.1}\text{O}_{3-\delta}$ . The results showed that  $\text{BaCo}_{0.7}\text{Fe}_{0.2}\text{Nb}_{0.1}\text{O}_{3-\delta}$  had a high oxygen permeation flux and good chemical stability in real operating condition. Cheng *et al.* [18] reported that  $\text{BaCo}_{0.7}\text{Fe}_{0.2}\text{Nb}_{0.1}\text{O}_{3-\delta}$  was a p-type semiconductor and has a good stability in reducing atmosphere. The reaction was processed in the partial oxidation of methane reactor with the oxygen permeation flux of  $25.77 \text{ ml}\cdot\text{min}^{-1}\cdot\text{cm}^{-2}$  at  $875^\circ\text{C}$  using the membrane with the thickness of 1 mm. Zhang *et al.* [19] reported that  $\text{BaCo}_{0.7}\text{Fe}_{0.2}\text{Nb}_{0.1}\text{O}_{3-\delta}$  had a high stability to withstand the harsh reduction condition. Zhu *et al.* [20] reported that  $\text{BaCo}_{0.7}\text{Fe}_{0.2}\text{Nb}_{0.1}\text{O}_{3-\delta}$  is a promising cathode materials because it exhibited the low polarized resistance of  $0.0082 \Omega\text{cm}^2$  at  $800^\circ\text{C}$ . Zhang *et al.* [21] used Ru-based catalyst on top of  $\text{BaCo}_{0.7}\text{Fe}_{0.2}\text{Nb}_{0.1}\text{O}_{3-\delta}$  in order to improve the oxygen permeation flux of the membrane, and tested the membrane in the production of syngas ( $2\text{CH}_4 + \text{O}_2 \rightarrow 2\text{CO} + 4\text{H}_2$ ). The feed gas, methane, was obtained as a byproduct from the process of producing coke from coal at high temperature of  $800^\circ\text{C}$  and was contaminated with other gaseous by-products. They found that the membrane had high stability to the atmospheric condition of partial oxidation of methane. Cheng *et al.* [22] applied  $\text{BaCo}_{0.7}\text{Fe}_{0.2}\text{Nb}_{0.1}\text{O}_{3-\delta}$  as the permeation membrane materials for partial oxidation of toluene.

### 1.3 Literature review of catalyst materials

In order to enhance the oxygen permeation flux of oxygen permeation membranes, the membrane might be coated with selected catalysts to enhance the adsorption and desorption capacities on the surface. Therefore, oxygen sorption/desorption property and structural stability become the crucial factors.

#### 1.3.1 SCF

Ma *et al.* [23] investigated the structure and phase stability of  $\text{SrCoFe}_{0.5}\text{O}_x$  under reducing environment.  $\text{SrCoFe}_{0.5}\text{O}_x$  obtained as a mixture of three phases;  $\text{Sr}_4\text{Fe}_{6-x}\text{Co}_x\text{O}_{13\pm\delta}$ ,  $\text{SrFe}_{1-x}\text{Co}_x\text{O}_{3-\delta}$  and  $\text{Co}_{3-x}\text{Fe}_x\text{O}_4$  exhibited structural stability at high temperature and had a high electrical conductivity. Yin *et al.* [24] also reported that  $\text{SrCoFeO}_x$  consisted of three phases similar to that reported by Ma *et al.* Moreover, they investigated the oxygen adsorption and desorption of  $\text{SrCoFeO}_x$  and found that  $\text{SrCoFeO}_x$  had a larger oxygen sorption capacity ( $\sim 0.41$  mmol/g for SCF and  $\sim 0.28$  mmol/g for LSCF at  $800^\circ\text{C}$ ) and stronger phase stability than  $\text{La}_{0.1}\text{Sr}_{0.9}\text{Co}_{0.9}\text{Fe}_{0.1}\text{O}_{3-\delta}$ . Because  $\text{Sr}_4\text{Fe}_{6-x}\text{Co}_x\text{O}_{13\pm\delta}$  phase in  $\text{SrCoFeO}_x$  is defined by alternating perovskite-like and rock-salt-like layers and these rock-salt-like layers are able to adsorb oxygen at high oxygen partial pressure [24]. Kim *et al.* [25] studied oxygen permeation kinetics of  $\text{SrCoFe}_{0.5}\text{O}_{3.25-\delta}$  and found that the oxygen transport was controlled by bulk diffusion rate.

#### 1.3.2 LSCF

Yang *et al.* [26] studied the oxygen adsorption desorption of  $\text{La}_{0.1}\text{Sr}_{0.9}\text{Co}_{0.9}\text{Fe}_{0.1}\text{O}_{3-\delta}$  in a fixed bed system ceramic sorbent and found that it gave high oxygen capacity (0.247 mmol/g at  $800^\circ\text{C}$ ) and fast oxygen sorption rate. Moreover, it exhibited good reversibility and stability for oxygen sorption and desorption. Kusaba *et al.* [27] investigated the contribution of surface reaction and bulk diffusion in oxygen permeation phenomena of  $\text{La}_{0.1}\text{Sr}_{0.9}\text{Co}_{0.9}\text{Fe}_{0.1}\text{O}_{3-\delta}$ . It was found that  $\text{La}_{0.1}\text{Sr}_{0.9}\text{Co}_{0.9}\text{Fe}_{0.1}\text{O}_{3-\delta}$  had a good oxygen adsorption rate.

### 1.3.3 SCFN

He *et al.* [28] studied the effect of dopant on the oxygen desorption and oxygen permeability of  $\text{SrCo}_{0.4}\text{Fe}_{0.5}\text{M}_{0.1}\text{O}_{3-\delta}$  (M = Ni, Al and Zr). The result showed that  $\text{SrCo}_{0.4}\text{Fe}_{0.5}\text{Ni}_{0.1}\text{O}_3$  has higher  $\alpha$ -oxygen desorption (about 1.43 times) than  $\text{SrCo}_{0.4}\text{Fe}_{0.6}\text{O}_3$ . The amounts of  $\alpha$ -oxygen (oxygen in the intrinsic oxygen vacancies of the materials) desorption exhibited the following order:  $\text{SrCo}_{0.4}\text{Fe}_{0.5}\text{Ni}_{0.1}\text{O}_{3-\delta} > \text{SrCo}_{0.4}\text{Fe}_{0.5}\text{Al}_{0.1}\text{O}_{3-\delta} \approx \text{SrCo}_{0.4}\text{Fe}_{0.6}\text{O}_{3-\delta} > \text{SrCo}_{0.4}\text{Fe}_{0.5}\text{Zr}_{0.1}\text{O}_{3-\delta}$ , and the oxygen permeation flux arranged as  $\text{SrCo}_{0.4}\text{Fe}_{0.5}\text{Ni}_{0.1}\text{O}_{3-\delta} > \text{SrCo}_{0.4}\text{Fe}_{0.6}\text{O}_{3-\delta} > \text{SrCo}_{0.4}\text{Fe}_{0.5}\text{Zr}_{0.1}\text{O}_{3-\delta} > \text{SrCo}_{0.4}\text{Fe}_{0.5}\text{Al}_{0.1}\text{O}_{3-\delta}$ . Because doping with low valence metal ions ( $\text{Ni}^{2+}$ ) can increase oxygen vacancy concentration, the amount of  $\alpha$ -oxygen desorption was increased.

## 1.4 Literature review of surface modification

Wang *et al.* [29] investigated the oxygen permeation flux of  $\text{Ba}_{0.5}\text{Sr}_{0.5}\text{Co}_{0.8}\text{Fe}_{0.2}\text{O}_{3-\delta}$  membrane coated with  $\text{GdBaCo}_2\text{O}_{5+\delta}$  in the temperature range of 600 - 850°C. The results showed that the  $\text{GdBaCo}_2\text{O}_{5+\delta}$  coated on a permeation side (He side) had greater effect than that coated on the air side. At 850°C, the oxygen permeation flux of  $\text{Ba}_{0.5}\text{Sr}_{0.5}\text{Co}_{0.8}\text{Fe}_{0.2}\text{O}_{3-\delta}$  membrane coated by  $\text{GdBaCo}_2\text{O}_{5+\delta}$  on the air side, He side and both sides were 16%, 27% and 41% higher than the flux of uncoated  $\text{Ba}_{0.5}\text{Sr}_{0.5}\text{Co}_{0.8}\text{Fe}_{0.2}\text{O}_{3-\delta}$  membrane, respectively. Shen *et al.* [30] studied the effect of coating layer of  $\text{RBaCo}_2\text{O}_{5+\delta}$  (R = Pr, Nd, Sm and Gd) on the oxygen permeation flux through  $\text{Ba}_{0.5}\text{Sr}_{0.5}\text{Co}_{0.8}\text{Fe}_{0.2}\text{O}_{3-\delta}$  membrane. As a result, the oxygen permeation flux of the membrane increased after coating with the catalyst layer. Lee *et al.* [31] investigated the enhancement of oxygen permeation by  $\text{La}_{0.6}\text{Sr}_{0.4}\text{CoO}_{3-\delta}$  coating on  $\text{La}_{0.7}\text{Sr}_{0.3}\text{Ga}_{0.6}\text{Fe}_{0.4}\text{O}_{3-\delta}$  membrane, and found that the oxygen permeation flux of coated membrane increased 2 – 6 times higher than the flux of uncoated membrane.

From the reviews above,  $\text{Ba}_{0.5}\text{Sr}_{0.5}\text{Co}_{0.8}\text{Fe}_{0.2}\text{O}_3$  and  $\text{BaCo}_{0.7}\text{Fe}_{0.2}\text{Nb}_{0.1}\text{O}_3$  have good mixed ionic and electronic conductivity and high oxygen permeation flux, which are suitable for oxygen permeation membrane.  $\text{SrCoFeO}_x$ ,  $\text{La}_{0.1}\text{Sr}_{0.9}\text{Co}_{0.9}\text{Fe}_{0.1}\text{O}_3$  and

$\text{SrCo}_{0.4}\text{Fe}_{0.5}\text{Ni}_{0.1}\text{O}_3$  have good oxygen adsorption and desorption properties, which are suitable for catalysts in oxygen permeation separator.

In this thesis, the oxygen permeation of  $\text{BaCo}_{0.7}\text{Fe}_{0.2}\text{Nb}_{0.1}\text{O}_3$  (BCFN) and  $\text{Ba}_{0.5}\text{Sr}_{0.5}\text{Co}_{0.8}\text{Fe}_{0.2}\text{O}_3$  (BSCF) coated with  $\text{SrCoFeO}_x$  (SCF),  $\text{La}_{0.1}\text{Sr}_{0.9}\text{Co}_{0.9}\text{Fe}_{0.1}\text{O}_3$  (LSCF) and  $\text{SrCo}_{0.4}\text{Fe}_{0.5}\text{Ni}_{0.1}\text{O}_3$  (SCFN) as catalyst layers were investigated. In addition, the chemical compatibility of membranes and catalysts and the long-term stability of double-coated membranes were investigated.

### **1.5 The objectives of this study**

To enhance the oxygen permeation flux of  $\text{BaCo}_{0.7}\text{Fe}_{0.2}\text{Nb}_{0.1}\text{O}_3$  (BCFN) and  $\text{Ba}_{0.5}\text{Sr}_{0.5}\text{Co}_{0.8}\text{Fe}_{0.2}\text{O}_3$  (BSCF) membranes by coating with the catalysts of  $\text{SrCoFeO}_x$  (SCF),  $\text{La}_{0.1}\text{Sr}_{0.9}\text{Co}_{0.9}\text{Fe}_{0.1}\text{O}_3$  (LSCF) and  $\text{SrCo}_{0.4}\text{Fe}_{0.5}\text{Ni}_{0.1}\text{O}_3$  (SCFN) and study for the stability of modified membranes.

## CHAPTER II

### THEORY

#### 2.1 Oxygen separation from air using Ceramic membranes

There are two oxygen separation systems of ceramic membrane distinguished by the type of membranes, pure oxygen conducting membranes and mixed ionic-electronic conducting (MIEC) membranes. The first system using pure oxygen conducting membrane requires an external circuit and electrodes for electron pathway as illustrated in figure 2.1 a). The latter system, based on MIEC materials, requires neither an electrode nor an external circuit but the system needs the oxygen pressure difference on both sides of the membrane as shown in figure 2.1 b) [4-5]. Figure 2.1 b(i) is the ideal mixed ionic and electronic conducting membrane. This membrane consists of one phase which is capable for both ionic and electronic conduction. Figure 2.1b(ii) is the dual phase of mixed ionic and electronic conducting membrane which consists of predominantly ionic conducting phase and superior electron conducting phase.

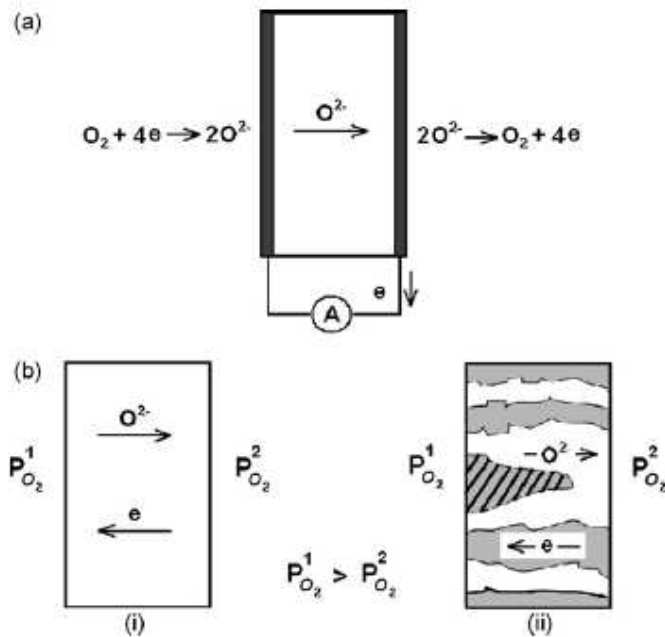


**Figure 2.1** Types of oxygen separation system; a) pure oxygen conducting membrane, and b) mixed ionic electronic (i) single phase conducting membrane and (ii) dual phase conducting membrane [4].

The method for separation oxygen from air by dense MIEC ceramic membrane has been widely investigated because it produces high purity oxygen and requires neither an electrode nor an external circuit. The separation of oxygen from air was carried out at typically 800 – 900°C and the oxygen permeates from the high oxygen partial pressure side (air side) to the low oxygen partial pressure side (He side) [4]. From figure 2.2 at the air side, oxygen is adsorbed on the membrane surface and is reduced by active sites of the membrane to become oxide ions. The oxide ion migrates through membrane to the He side where the oxidation reaction occurs and produces oxygen gas and electrons. Electrons move to the air side to balance the charge of membrane.

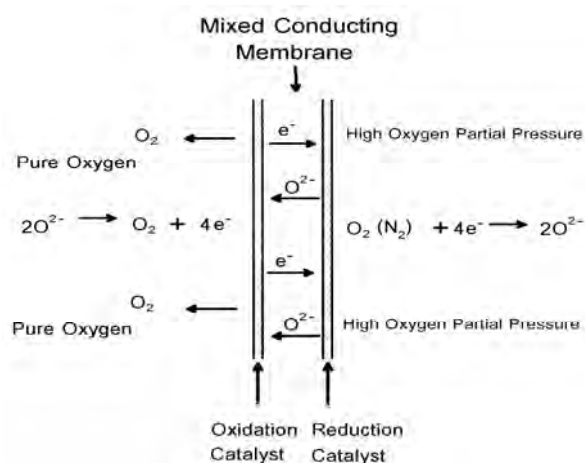


**Figure 2.2** Schematic representation of the oxygen transport through mixed conducting membrane [32].

## 2.2 Perovskite structure

There are many structures used as ceramic membranes such as fluorite, pyrochlore, brownmillerite,  $K_2NiF_4$ -typed structure and perovskite. Most compounds showing good oxygen permeation properties are fluorite and perovskite. This work is interested in the perovskite structure. The crystal structure of the ideal perovskite is in a cubic system with a simple formula of  $ABO_3$  ( $A^{1+}B^{5+}O_3$ ,  $A^{2+}B^{4+}O_3$  and  $A^{3+}B^{3+}O_3$ ) as shown in figure 2.3. The A symbol is a large size cation, the B symbol is a medium size cation and the O symbol is an oxide ion. The A cations are located at the corners of cubic and the B cations are located at the center, while the O anions are located at the center of the cubic face. The A cations and O anions form the  $AO_6$  octahedral

which exhibits  $90^\circ$  angles and six equal A – O bonds. Each B cation is surrounded by twelve O anions [5].

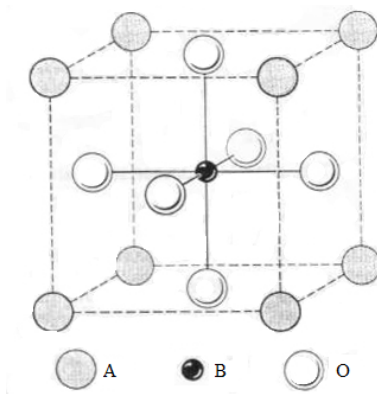


**Figure 2.3** Simple drawing of perovskite structure ( $ABO_3$ ) [33].

## 2.3 Ceramic compounds preparation methods

### *Conventional powder methods*

Solid-state reaction is a conventional method to synthesize metal oxide powders. The carbonates, hydroxides, nitrates, sulfates, acetates, oxalates, alkoxides, and other metal salts are commonly used as the reactants. The reactants are ground to well-mixed and then fired at high temperature about two third of the melting point for several hours to produce the desired product. Eventhough this method use high temperature and long time period and may result in mixed phases, it is usually tried first because the procedure is easy and the reactants are relatively cheaper [5, 34].

### *Co-precipitation*

This method starts from an aqueous solution which consists of desired cations, then a precipitation agent is added to the mixture. The precipitates are then followed by filtration, drying and thermal decomposition. The purity and properties of desired product are controlled by pH, mixing rates, temperature and concentration. An advantage of this method is to achieve fine powders by using lower calcination temperature. Also the reactants are relatively cheaper than other unconventional methods. However, the difference in the solubility of reactants in the solution plays an important factor to obtain a single-phased product [5, 34].

### *Sol-gel synthesis*

This technique involves the creation of “sol” from the solution of desired cations by the hydrolysis and condensation processes until the mixture becomes an amorphous-like gel. Then the solvent and by-products were removed from gel and the crystallized powder is the final product at medium temperature. An advantage of this method is that the homogeneity of cationic reactants on an atomic level could be achieved and monodispersed powders could be obtained. However, the reactants, usually metal organic compounds, are expensive and easily decomposed [5, 34].

### *Solvothermal synthesis*

Solvothermal or hydrothermal synthesis is the method which involves heating the reactants in liquid/solvent steam at high pressures and temperatures. The reactant and solvent are placed inside a Teflon-lined cylinder which is either sealed or connected to an external pressure control. An advantage of this method is the low reaction temperature about 100 – 500°C. However, the complication arises from the uncontrolled seeding and precipitation rate at fluctuated temperature and pressure [34].

### *Combustion synthesis*

This method is also known as self-propagating high temperature synthesis and solid state metathesis. It involves highly exothermic and explosive reaction to keep a self-propagating high reaction temperature. The starting materials are mixed together and then ignited to high temperature. The reaction propagates as a wave through the mixture and keep temperature about 3000°C during the fast reaction. Advantages of this method are possibility in using various kinds of reactant, yield high purity products and small particle size of product. The homogeneous solution of cationic reactants can be prepared on an atomic level. The drawback would be the requirement of fuel and oxidant for self combustion [34].

## **2.4 Powder compacting by uniaxial pressing**

The objective of the pressing step is to achieve maximum particle packing and uniformity. The primary driving force for densification of a compacted powder at high temperature is the change in surface free energy. The high surface free energy and very strong thermodynamic drive force decrease the surface by bonding them



together. Uniaxial pressing involves the compaction of powder in a rigid die by applying pressure in a single axial direction through a rigid punch or piston. The presses are usually mechanical or hydraulic. Pressing results in the direct contact of particles, reduces the average distance between particles, and changes the shape of particles. To enhance the compaction, before pressing, the powder should be disaggregated by mixing the powder with solvent such as isopropanol in the ultrasonic bath or adding a couple drops of acetone to reduce the surface tension.

## 2.5 Sintering

Sintering is a process of permanent chemical and physical change by decreasing the porosity by the grain growth at high temperature. When an aggregated powder is sintered, necks of interagglomerate are formed between the particles, and the density of the aggregate increases. The growth of the neck increases with the transport of matter or the counter-flow of vacancies between particles and pores. The sintering process can be divided into three stages.

The first stage is the formation of necks at points of particle contact. At this stage the individual particles are still distinguishable. The second stage is that the necks become large, resulting in the formation of an interconnected pore structure. The third stage, the pores become isolated. The interconnectivity of pores eliminates surface and vapor transport [35].

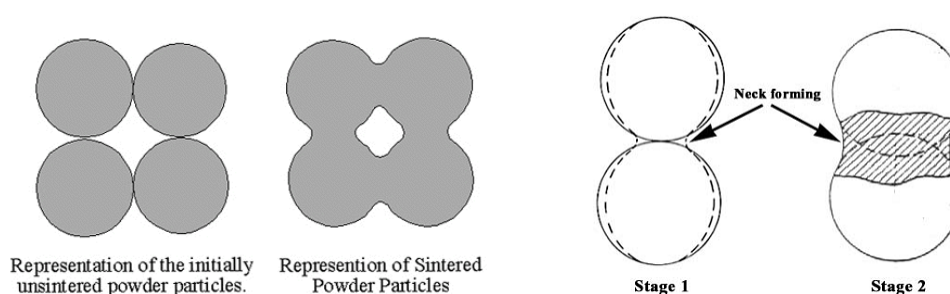


**Figure 2.4** Mechanism of sintering [36].

## 2.6 Phase characterization of materials

X-ray diffraction (XRD) is one of the physical methods normally used for phase purity analysis and structure determination of crystalline solids [37]. The most important theory in XRD would be the Bragg equation:

$$n\lambda = 2d\sin\theta \quad (2.12)$$

Where  $d$  is an interplanar spacing between the crystal planes,  $n$  is an integer,  $\lambda$  is the wavelength of the X-rays, and  $\theta$  is the diffraction angle.  $\lambda$  and  $d$  are measured in the same units, usually in angstroms.

The technique is widely used because the ease of sample preparation which is in the form of fine powders. The powder sample contains very small crystallites with random orientations. Therefore, when an X-ray beam strikes a powder sample, it is diffracted various sets of crystal spacings in the directions that governed by Bragg equation, resulting to the specific pattern that relates diffraction angles and diffracted intensities.

All crystalline solids have a unique diffraction pattern and there are 150,000 unique powder diffraction data collected in the database known as the JCPDS (Joint Committee on Powder Diffraction Standard). Therefore, the experimental diffraction data can be cross-matched for both the positions and intensities.

In order to go further to structural determination, the Miller indices can be determined using the relationship between the diffraction angles and lattice parameters. For example, the relationship between the diffraction angles, Miller indices and lattice parameters of a cubic crystal system is represented in equation 2.13.

$$\sin^2 \theta = \frac{\lambda^2}{4a^2} (h^2 + k^2 + l^2) \quad (2.13)$$

The  $\lambda$  and  $a$  are constant. If the first reflection is at an angle  $2\theta_1$  with Miller indices of  $h_1$ ,  $k_1$  and  $l_1$  then the relationship between the diffraction angles, Miller indices and lattice parameters can be write as equation 2.14

$$\sin^2 \theta_1 = \frac{\lambda^2}{4a^2} (h_1^2 + k_1^2 + l_1^2) \quad (2.14)$$

Dividing equation 2.13 by equation 2.14 and then give the equation 2.15

$$\frac{\sin^2 \theta}{\sin^2 \theta_1} = \frac{(h^2 + k^2 + l^2)}{(h_1^2 + k_1^2 + l_1^2)} \quad (2.15)$$

The first reflection for the primitive lattice is 100. Therefore it can rewrite the equation 2.15 as equation 2.16.

$$\frac{\sin^2 \theta}{\sin^2 \theta_1} = \frac{(h^2 + k^2 + l^2)}{1^2} \quad (2.16)$$

In similar manner  $h$ ,  $k$  and  $l$  for all reflections can be calculated. After that, the lattice parameter,  $a$ , is calculated by using the known values ( $\theta$ ,  $\lambda$ ,  $h$ ,  $k$  and  $l$ ) of each reflection with equation 2.13.

In the case of other structure systems, equation 2.14 becomes more complicated as the number of variations (lattice constants) increases [38].

## 2.7 Oxygen transport

For dense mixed ionic-electronic conducting membranes, there are three steps involved in the oxygen transport mechanism as shown in figure 2.5. First step is the surface-exchange reaction on high oxygen partial pressure interface. The second is the oxide ion and electron transport simultaneously through the bulk phase. The last is surface-exchange reaction on low oxygen partial pressure interface. In these three steps, the slowest step is the rate determining step which may be considered in two cases, bulk-diffusion limit and surface-exchange limit. The rate determination step can be roughly predicted from the thickness of membranes, as shown in figure 2.6, that the transport through thick membranes is controlled by bulk-diffusion, while the transport through thin membranes is controlled by surface-exchange reaction [5].

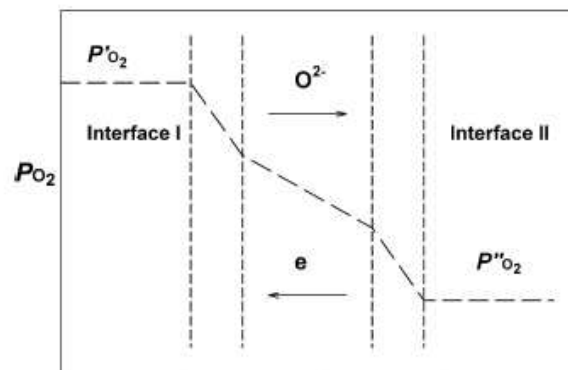


**Figure 2.5** Different sections involved in oxygen transport during oxygen permeation [5].

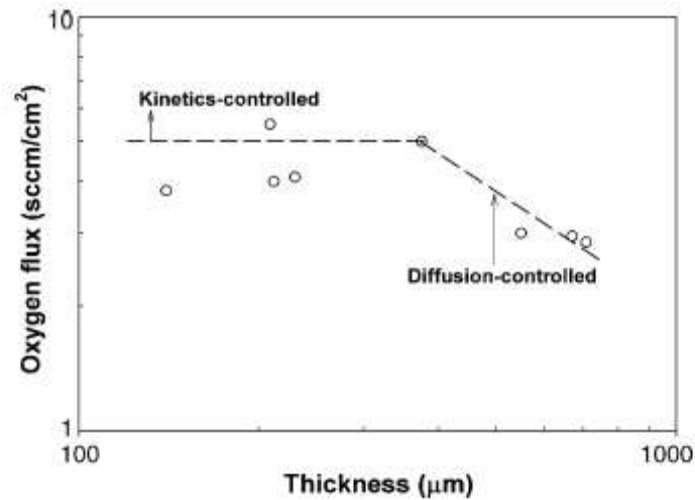


**Figure 2.6** Variation of regime from bulk-diffusion to surface-exchange reaction relevant to membrane thickness [5].

### 2.7.1 Bulk-diffusion limited

In the case that the oxygen permeation flux of ceramic membranes was controlled by bulk-diffusion, it is generally described by Wagner's equation which is shown in equation 2.23 [39-40].

$$J_{O_2} = -\frac{RT}{4^2 F^2 L} \int_{\ln P_{O_2}'}^{\ln P_{O_2}''} t_{el} \sigma_{ion} d \ln P_{O_2} \quad 2.23$$

- When
- $J_{O_2}$  is Oxygen permeation flux.
  - $P_{O_2}'$  is oxygen partial pressure at supply side.
  - $P_{O_2}''$  is oxygen partial pressure at permeate side.
  - R is gas constant.
  - $t_{el}$  is the electronic transference number.
  - $\sigma_{ion}$  is the ionic conductivity.
  - L is the membrane thickness.

From equation 2.23, the oxygen permeation flux depends on both ionic and electronic diffusions.

### 2.7.2 Surface-exchange limited

In the case that the surface-exchange reaction rate becomes the limiting step in the oxygen permeation, the Wagner equation is not applicable. In order to explain the oxygen permeation flux, the mechanisms below were proposed.



If the slowest moving species is  $O^x$  in the interface I, the concentration of species  $O^x$  can write as equation 2.30.

$$[O_{(w')}^x] = \frac{K_{O_{(w')}^x} K_{O_{(w')} }^{1/2} [V_{O(w')}] p_{O_2}^{1/2}}{p_{(w')}} \quad (2.30)$$

Where

$$K_{O_{(w')}} = \frac{O_{(w')}^2}{p_{O_2(g')}} \quad (2.31)$$

$$K_{O_{(w')}^x} = \frac{[O_{(w')}^x] p_{(w')}}{[O_{(w)}][V_{O(w)}]} \quad (2.32)$$

If the oxygen permeation flux is proportional to the concentration of species  $O^x$  and assuming that the concentration of all other oxygen species including electron holes are much higher and can be taken as constant, then the oxygen permeation flux can be written as equation 2.33[5].

$$J_{O_2} = \alpha (p_{O_2}^{1/2} - p'_{O_2}^{1/2}) \quad (2.33)$$

## 2.8 Oxygen permeation flux

According to Knudsen diffusion mechanism, the relation between the flux of leaked  $N_2$  and leaked  $O_2$  can write in equation 2.34 [9].

$$J_{N_2}^{leak}; J_{O_2}^{leak} = \sqrt{(32/38)} \times 0.79 : 0.21 \quad (2.34)$$

Therefore the oxygen permeation flux can calculated using equation 2.35

$$J_{O_2} = \left[ C_{O_2} - C_{N_2} \times \frac{0.21}{0.79} \times \left( \frac{28}{32} \right)^{\frac{1}{2}} \right] \times \frac{F}{S} \quad (2.35)$$

Where,  $C_{O_2}$  is the measured concentration of oxygen in the gas on the sweep side.

$C_{N_2}$  is the measured concentration of nitrogen in the gas on the sweep side.

F is the flow rate of the exit gas on the sweep side.

S is the membrane geometric surface area of the sweep side.

## CHAPTER III

### EXPERIMENTAL

#### 3.1 Chemicals

All chemicals listed in table 3.1 were used without further purification.

**Table 3.1** The detailed list of chemicals and reagents

Reagent	Formula weight	Purity (%)	Company
BaCO <sub>3</sub>	197.37	≥98.5	Sigma-Aldrich
SrCO <sub>3</sub>	147.63	≥99.9	Aldrich
CoO	74.93	95	BDH
Co <sub>3</sub> O <sub>4</sub> , powder	240.80	-	Aldrich
Fe <sub>2</sub> O <sub>3</sub>	159.68	≥99.0	Fluka
Nb <sub>2</sub> O <sub>5</sub>	265.81	99.99	Aldrich
La(NO <sub>3</sub> ) <sub>3</sub> ·6H <sub>2</sub> O	433.02	≥99.0	Fluka
Sr(NO <sub>3</sub> ) <sub>2</sub>	211.63	≥99.0	Fluka
Co(NO <sub>3</sub> ) <sub>2</sub> ·6H <sub>2</sub> O	291.03	98	Aldrich
Fe(NO <sub>3</sub> ) <sub>3</sub> ·9H <sub>2</sub> O	404.00	99 – 101	Fluka
Ni(NO <sub>3</sub> ) <sub>2</sub> ·6H <sub>2</sub> O	290.81	97.0	Ajax
HNO <sub>3</sub>	63.01	65	Merck
NH <sub>4</sub> OH	35.05	30	Panreac
Citric acid	192.13	99.5 – 100.5	Riedel-de Haën
n-butyl acetate	116.16	99.5	Carlo Erba
ZrO <sub>2</sub> – 8% Y <sub>2</sub> O <sub>3</sub>	-	99.9	Aldrich

#### 3.2 Synthesis of materials

The synthesis of materials consists of two parts, membrane materials and catalyst materials.

##### *Membrane materials:*

##### **3.2.1 Preparation of Ba<sub>0.5</sub>Sr<sub>0.5</sub>Co<sub>0.8</sub>Fe<sub>0.2</sub>O<sub>3</sub> membrane**

Ba<sub>0.5</sub>Sr<sub>0.5</sub>Co<sub>0.8</sub>Fe<sub>0.2</sub>O<sub>3</sub> (BSCF) was prepared by solid state method with the starting materials of BaCO<sub>3</sub>, SrCO<sub>3</sub>, CoO and Fe<sub>2</sub>O<sub>3</sub>. The stoichiometric mixture of metal mole ratio of starting materials was grinded for 30 min, and then calcined at 900°C for 5 h with the heating and cooling rates of 200°C·h<sup>-1</sup>. The obtained powder was grinded again and pressed into a disk with a diameter of 20 mm under a uniaxial pressure of 20 MPa for 5 min, followed by an isostatic pressure of 40 MPa for 20 min. The disk was sintered at 1200°C for 5 h with the heating and cooling rates of 200°C·h<sup>-1</sup>.

<sup>1</sup> up to 1000°C, then of 100°C·h<sup>-1</sup> above 1000°C. The dense membrane of BSCF was polished until the thickness of membrane was about 0.5 mm.

### 3.2.2 Preparation of BaCo<sub>0.7</sub>Fe<sub>0.2</sub>Nb<sub>0.1</sub>O<sub>3</sub> membrane

BaCo<sub>0.7</sub>Fe<sub>0.2</sub>Nb<sub>0.1</sub>O<sub>3</sub> (BCFN) was prepared by solid state method with the starting materials of BaCO<sub>3</sub>, Co<sub>3</sub>O<sub>4</sub>, Fe<sub>2</sub>O<sub>3</sub> and Nb<sub>2</sub>O<sub>5</sub>. The stoichiometric mixture of metal mole ratio of starting materials was grinded for 30 min, and then calcined at 1100°C for 20 h with the heating and cooling rates of 120°C·h<sup>-1</sup>. The obtained powder was grinded again and pressed into a disk with a diameter of 20 mm under a uniaxial pressure of 48 MPa for 10 min. The disk was sintered at 1150°C for 20 h with the heating and cooling rates of 60°C·h<sup>-1</sup>. The dense membrane of BCFN was polished until the thickness of membrane was about 0.5 mm.

#### *Catalyst materials:*

### 3.2.3 Synthesis of La<sub>0.1</sub>Sr<sub>0.9</sub>Co<sub>0.9</sub>Fe<sub>0.1</sub>O<sub>3</sub>

La<sub>0.1</sub>Sr<sub>0.9</sub>Co<sub>0.9</sub>Fe<sub>0.1</sub>O<sub>3</sub> (LSCF) was synthesized by a modified citrate method with the starting materials of La(NO<sub>3</sub>)<sub>3</sub>·6H<sub>2</sub>O, Sr(NO<sub>3</sub>)<sub>2</sub>, Co(NO<sub>3</sub>)<sub>2</sub>·6H<sub>2</sub>O and Fe(NO<sub>3</sub>)<sub>3</sub>·9H<sub>2</sub>O. The stoichiometric mixture of metal mole ratio of starting materials was dissolved in water and nitric acid. The solution was stirred for 3 h, then citric acid was added with the ratio of citric acid : total metal of 2 : 1. The mixture solution was stirred for another 3 h. NH<sub>4</sub>OH was slowly added until the pH of solution reached 9 – 10. Then the solution was stirred overnight. After that, the solution was heated to self-ignite and became powder. The obtained powder was calcined for 5 h at 950°C with the heating and cooling rates of 200°C·h<sup>-1</sup>.

### 3.2.4 Synthesis of SrCoFeO<sub>x</sub>

SrCoFeO<sub>x</sub> (SCF) was synthesized by a modified citrate method with the starting materials of Sr(NO<sub>3</sub>)<sub>2</sub>, Co(NO<sub>3</sub>)<sub>2</sub>·6H<sub>2</sub>O and Fe(NO<sub>3</sub>)<sub>3</sub>·9H<sub>2</sub>O. The stoichiometric mixture of metal mole ratio of starting materials was dissolved in water and nitric acid. The solution was stirred for 3 h, then citric acid was added with the ratio of citric acid : total metal of 2 : 1. The mixture solution was stirred for another 3 h. NH<sub>4</sub>OH was slowly added until the pH of solution reached 9 – 10. Then the



solution was stirred overnight. After that, the solution was heated to self-ignite and became powders. The obtained powder was calcined for 5 h at 900°C with the heating and cooling rates of 200°C·h<sup>-1</sup>.

### **3.2.5 Synthesis of SrCo<sub>0.4</sub>Fe<sub>0.5</sub>Ni<sub>0.1</sub>O<sub>3</sub>**

SrCo<sub>0.4</sub>Fe<sub>0.5</sub>Ni<sub>0.1</sub>O<sub>3</sub> (SCFN) was synthesized by a modified citrate method with the starting materials of Sr(NO<sub>3</sub>)<sub>2</sub>, Co(NO<sub>3</sub>)<sub>2</sub>·6H<sub>2</sub>O, Fe(NO<sub>3</sub>)<sub>3</sub>·9H<sub>2</sub>O and Ni(NO<sub>3</sub>)<sub>2</sub>·6H<sub>2</sub>O. The stoichiometric mixture of metal mole ratio of starting materials was dissolved in water and nitric acid. The solution was stirred for 3 h, then citric acid was added with the ratio of citric acid : total metal of 2 : 1. The mixture solution was stirred for another 3 h. NH<sub>4</sub>OH was slowly added until the pH of solution reached 9 – 10. Then the solution was stirred overnight. After that, the solution was heated to self-ignite and became powder. The obtained powder was calcined for 5 h at 950°C with the heating and cooling rates of 200°C·h<sup>-1</sup>.

## **3.3 Characterization of materials**

### **3.3.1 Powder X-ray diffraction (XRD)**

The crystal structures of BSCF, BCFN, LSCF, SCF and SCFN were characterized by X-ray diffraction (Rigaku, Dmax 2200/Ultima<sup>+</sup>) using Cu K $\alpha$  radiation. The tube voltage and current were set at 40 kV and 30 mA, respectively. Data were collected in the 2-theta range of 20 – 70 degree with the scan time of 0.5 s and the scan step of 0.020 degree. The scattering slit, divergent slit and receiving slit were fixed at 1 degree, 1 degree and 0.3 mm respectively.

### **3.3.2 Electrochemical impedance spectroscopy (EIS)**

To measure the conductivity of BSCF, the slurry of BSCF was prepared by mixing BSCF powder with a little amount of PEG and grinding for 10 min. The slurry was coated on both sides of ZrO<sub>2</sub> (8% Y<sub>2</sub>O<sub>3</sub>) dense membrane that was sintered at 1500°C for 5 h prior to the coating. The coated membranes were fired at 1000°C for 1 h in air to remove any organic component. The conductivity was measured using the ac impedance method performed on Solartron 1260 impedance/gain-phase analyzer over the frequency range of 0.05 Hz – 10 MHz in the temperature range of 300 –

900°C with heating rate of 180°C·h<sup>-1</sup> and the interval temperature of 50°C in air. Similar to BSCF, the conductivity of BCFN was performed in the same manner.

### 3.4 Catalytic coating

#### 3.4.1 Single-coating

BSCF and BCFN membranes with the thickness of 0.5 mm were coated by catalysts which were listed in Table 3.2. Catalyst powder was coated on either high oxygen partial pressure side (air side) or low oxygen partial pressure side (He side) of BSCF and BCFN membranes by screen-printing method. A little amount of n-butyl acetate was used as a binder for preparation of the catalyst slurry. The coated membrane was fired at 800°C for 10 min with the heating and cooling rates of 300°C·h<sup>-1</sup> to remove organic compounds and generate porous layer catalysts.

**Table 3.2** List of the catalytic coating on membranes

membrane	catalyst		codename
	air side	He side	
BSCF	SCF	-	SCF/BSCF
BSCF	LSCF	-	LSCF/BSCF
BSCF	SCFN	-	SCFN/BSCF
BSCF	-	SCF	BSCF/SCF
BSCF	-	LSCF	BSCF/LSCF
BSCF	-	SCFN	BSCF/SCFN
BCFN	SCF	-	SCF/BCFN
BCFN	LSCF	-	LSCF/BCFN
BCFN	SCFN	-	SCFN/BCFN
BCFN	-	SCF	BCFN/SCF
BCFN	-	LSCF	BCFN/LSCF
BCFN	-	SCFN	BCFN/SCFN

#### 3.4.2 Double-coating

The catalysts which gave the highest oxygen permeation flux for air side and He side were coated on air side and He side, respectively, for double-coating. Screen-printing method was applied for double-coating, using little amount of n-butyl acetate to make the catalyst slurry. The double-coated membrane was fired at 800°C for 10 min with the heating and cooling rates of 300°C·h<sup>-1</sup> to remove organic compounds and generate porous layer catalysts.

### 3.5 Oxygen permeation

The oxygen permeation flux was measured using the membrane reactor as represented in Figure 3.1. The membrane with the thickness of 0.5 mm was placed between two alumina tubes, which were sealed by two Pyrex rings. The ceramic tubular furnace ARF 30KC (Asahi Rika Seisakusho) and the temperature controller FCR-13A-R/M (Shinko) were used to adjust the reaction temperature. The connection between alumina tubes and membrane was completely sealed by the Pyrex ring heated at 1000°C. The upper side of the alumina tube was exposed to air-zero ( $21\pm 1\%$  O<sub>2</sub>) which was used as a feed gas, while the down side of the alumina tube was exposed to He (99.999%) which was used as a sweeping gas. The flow rates of air and He were controlled at 50 mL/min. The oxygen content of product stream was measured by a gas chromatography (HP 6820) in temperature range of 700 – 1000°C with the interval temperature of 100°C.

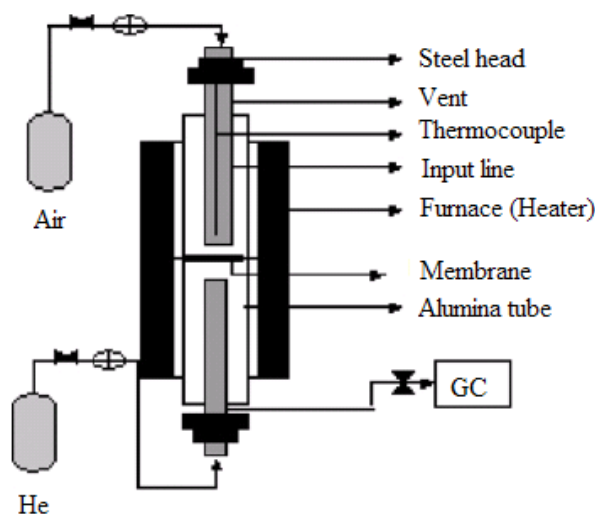


**Figure 3.1** Schematic diagram of the membrane reactor setup for oxygen permeation study [41].

### 3.6 Stability of coating-membranes

#### 3.6.1 Chemical compatibility of membranes and catalysts

The membranes coated by catalysts were tested for the chemical compatibility. If these two components react to each other at high temperature, the new phase(s) created at the interface can reduce the conductivity between membrane and catalysts. The chemical compatibility was studied using XRD and SEM/EDS techniques.

### ***Powder X-ray diffraction (XRD)***

BSCF was mixed with catalysts (LSCF, SCF or SCFN) in a 50/50 wt.%. The mixture was grinded, and then pressed into disk. The disk was heated from 800 – 1000°C with the interval temperature of 100°C. The phases of BSCF, catalyst and impurity were monitored by X-ray diffractometer. The compatibility of BCFN was performed in the same manner with BSCF.

### ***Scanning electron microscopy (SEM/EDS)***

Performed by JSM-6400 scanning electron microscope (JEOL Tokyo Japan), the morphology of catalysts on the disk membrane either before or after the oxygen permeation tests was captured by SEM. Furthermore the atomic diffusion across the interface between membranes and catalysts was monitored by SEM/EDS analysis. EDS analysis with an ID-point mode was used to determine the elements appeared on the cross-sectioned membrane/catalyst pellets.

### **3.6.2 Long-term oxygen permeation flux**

For practical application, the double-coating membranes need to be tested for the long-term oxygen permeation flux. The membrane reactor with double-coating of selected catalysts was operated at 850°C for 100 h and the oxygen content of the product stream was measured.

# CHAPTER IV

## RESULTS AND DISCUSSION

### 4.1 Synthesis and characterization

#### 4.1.1 Crystal structure of membrane materials

The XRD patterns of  $\text{Ba}_{0.5}\text{Sr}_{0.5}\text{Co}_{0.8}\text{Fe}_{0.2}\text{O}_3$  (BSCF) and  $\text{BaCo}_{0.7}\text{Fe}_{0.2}\text{Nb}_{0.1}\text{O}_3$  (BCFN) are shown in Figures 4.1 and 4.2 respectively. BSCF was prepared by solid state method with the calcination temperature of  $900^\circ\text{C}$  for 5h and the sintering temperature of  $1200^\circ\text{C}$  for 5h. The XRD pattern of BSCF indicates that a single-phased perovskite was achieved. The crystal structure of BSCF is in a cubic system which is similar to that of  $\text{Sr}(\text{Co}_{0.81}\text{Fe}_{0.19})\text{O}_{2.78}$  and  $\text{BaCoO}_{2.23}$  (JCPDS:82-2445 and JCPDS:75-0227, respectively) and that reported by Shao and co-workers [9] as shown in the appendix B Figure 1. BCFN was prepared by solid state method with the calcination temperature of  $1100^\circ\text{C}$  for 20h and the sintering temperature of  $1150^\circ\text{C}$  for 20h. Similar to BSCF, the XRD pattern of BCFN indicates a single-phased perovskite. The crystal structure of BCFN is in a cubic system which is similar to that of  $\text{Ba}(\text{Fe}_{0.33}\text{Nb}_{0.67})\text{O}_3$  and  $\text{Ba}_{0.9}\text{NbO}_3$  (JCPDS:17-0187 and JCPDS:80-2499, respectively) and that reported by Zhang and co-workers [19] as shown in the appendix B Figure 2.

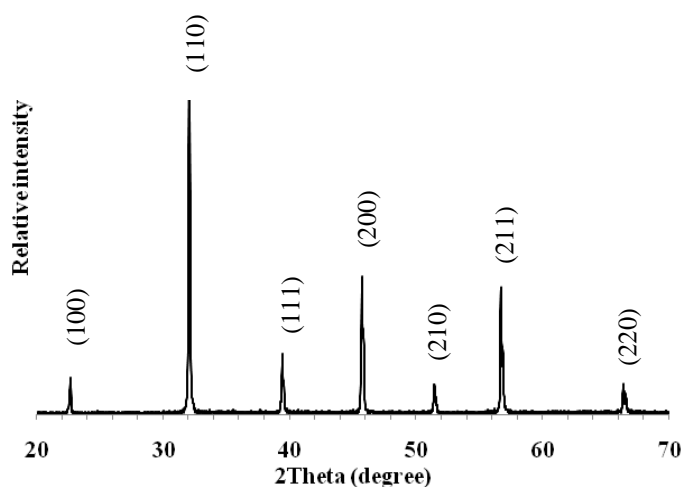


**Figure 4.1** XRD pattern of as-prepared BSCF.

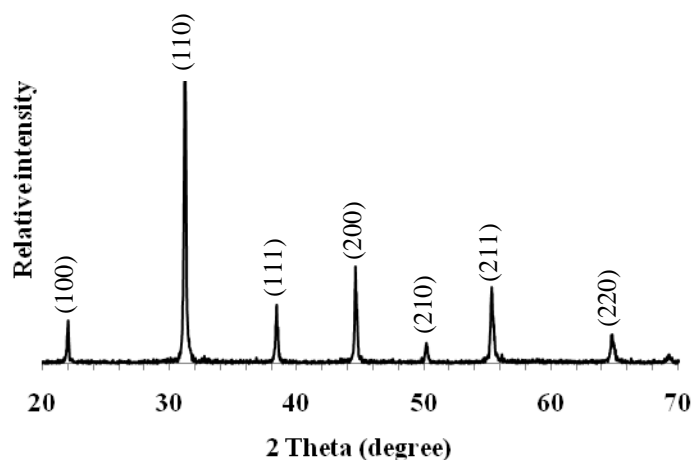


**Figure 4.2** XRD pattern of as-prepared BCFN.

The lattice parameters of BSCF, BCFN, LSCF and SCFN, showed in Table 4.1, were calculated from hkl of cubic system labeled in Figure 4.1 a), 4.2 a), 4.3 a) and 4.4 respectively. The densities of BSCF and BCFN membranes were measured by Archimedes' method and showed in Table 4.1. On the other hand the theoretical densities of the membranes were calculated from the five strongest peaks obtained from XRD patterns. The relative densities of BSCF and BCFN, as the ratio of Archimedes method density and theoretical density, were 88.57% and 79.28%, respectively. Because the relative density of BSCF was not much lower than the required density of 90%, its oxygen permeation property was studied.

**Table 4.1** Crystal structure, lattice parameters, density and relative density of BSCF, BCFN, LSCF, SCF and SCFN

Sample	Crystal structure	Lattice parameter, a(Å)	Density (g/cm <sup>3</sup> )	Theoretical density (g/cm <sup>3</sup> )	Relative density (%)
<b>Membrane</b>					
BSCF	Cubic	4.0043	5.04 ± 0.03	5.6586	88.57
BCFN	Cubic	4.0522	4.89 ± 0.01	6.1683	79.28
<b>Catalyst</b>					
LSCF	Cubic	3.7005			
SCF	Mixed phase	-			
SCFN	Cubic	3.8599			

#### 4.1.2 Crystal structure of catalyst materials

The XRD patterns of prepared  $\text{La}_{0.1}\text{Sr}_{0.9}\text{Co}_{0.9}\text{Fe}_{0.1}\text{O}_3$  (LSCF),  $\text{SrCo}_{0.4}\text{Fe}_{0.5}\text{Ni}_{0.1}\text{O}_3$  (SCFN) and  $\text{SrCoFeO}_x$  (SCF) are shown in Figures 4.3, 4.4 and 4.5, respectively. Catalyst materials were synthesized by modified citrate method with the calcination temperature of 950°C 5h for LSCF and SCFN and of 900°C 5h for SCF. The XRD pattern of prepared LSCF indicates that a single-phased perovskite was achieved. The crystal structure of LSCF is in a cubic system which is similar to that of  $\text{La}_{0.3}\text{Sr}_{0.7}\text{CoO}_3$  (JCPDS: 48-0137) and that of  $\text{La}_{0.1}\text{Sr}_{0.9}\text{Co}_{0.9}\text{Fe}_{0.1}\text{O}_3$  (LSCF1991) reported by Yin and co-workers [42] shown in the appendix B Figure 3. Similar to LSCF, the XRD pattern of prepared SCFN shows a single-phased perovskite. The crystal structure of SCFN is in a cubic system which is similar to that of  $\text{Sr}(\text{Co}_{0.5}\text{Fe}_{0.5})\text{O}_3$  (JCPDS:46-0335). On the contrary to the previous two catalysts, the prepared SCF in Figure 4.5, was not single-phased, but contained a perovskite phase ( $\text{SrCo}_{1-x}\text{Fe}_x\text{O}_3$ ) and a small amount of a spinel phase ( $\text{Co}_{3-x}\text{Fe}_x\text{O}_4$ ) and a layered-perovskite phase ( $\text{Sr}_4\text{Fe}_{6-x}\text{Co}_x\text{O}_{13}$ ). The prepared SCF mixed-phase is similar to that reported by Yin et al [24] shown in the appendix B Figure 4.

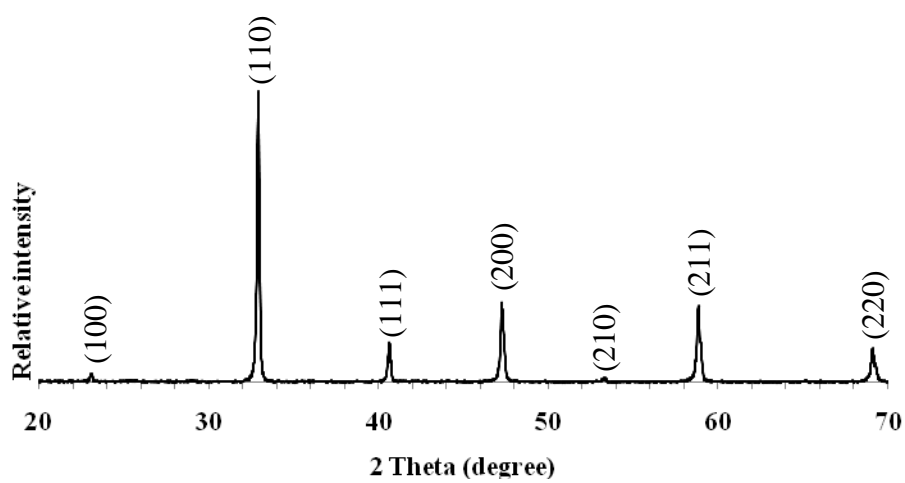


**Figure 4.3** XRD pattern of as-prepared LSCF.

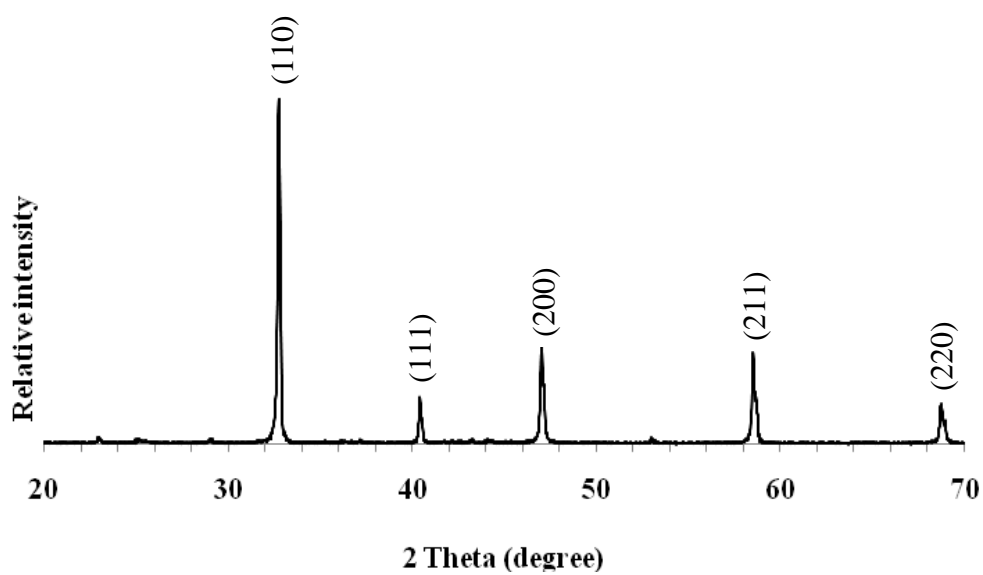


**Figure 4.4** XRD pattern of as-prepared SCFN.



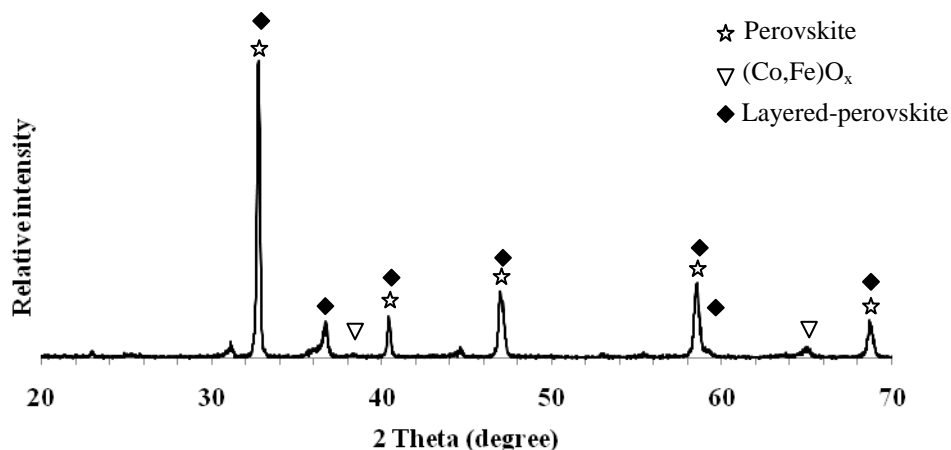


**Figure 4.5** XRD pattern of as prepared SCF.

#### 4.2 Conductivity of membranes

The materials used as a cathode for SOFC or a membrane for oxygen separation process must have high electrical conductivity. The oxygen permeation flux is maximum when the ionic and electronic transference numbers are equal, i.e. 0.5 [43]. In this work, the conductivity of BSCF and BCFN was studied using an AC-impedance technique. Figure 4.6 shows an Arrhenius plot between natural logarithm of conductivity and  $1000/\text{Temperature}$  of BSCF and BCFN perovskites. The conductivities of BSCF and BCFN take a similar increasing trend with increasing temperature. The conductivity of BSCF is higher than BCFN at all temperatures which is similar to that reported previously by Zhang et al. [17]. The Arrhenius plot shows that there are two slopes for both materials. It can be described that at temperature below  $550^\circ\text{C}$ , BSCF and BCFN are p-type semiconductors with electric holes as charge carriers. Above about  $550^\circ\text{C}$ , oxygen vacancies from lattice oxygen and electron holes are formed; therefore, the slope of an Arrhenius plot is changed. The Activation energy,  $E_a$ , was calculated from the slope of Arrhenius plot. At the temperature lower than  $550^\circ\text{C}$ , the  $E_a$  are 0.98 and 0.92 eV for BSCF and BCFN, respectively. At the temperature higher than  $550^\circ\text{C}$ , the  $E_a$  are 1.24 and 1.04 eV for BSCF and BCFN, respectively.

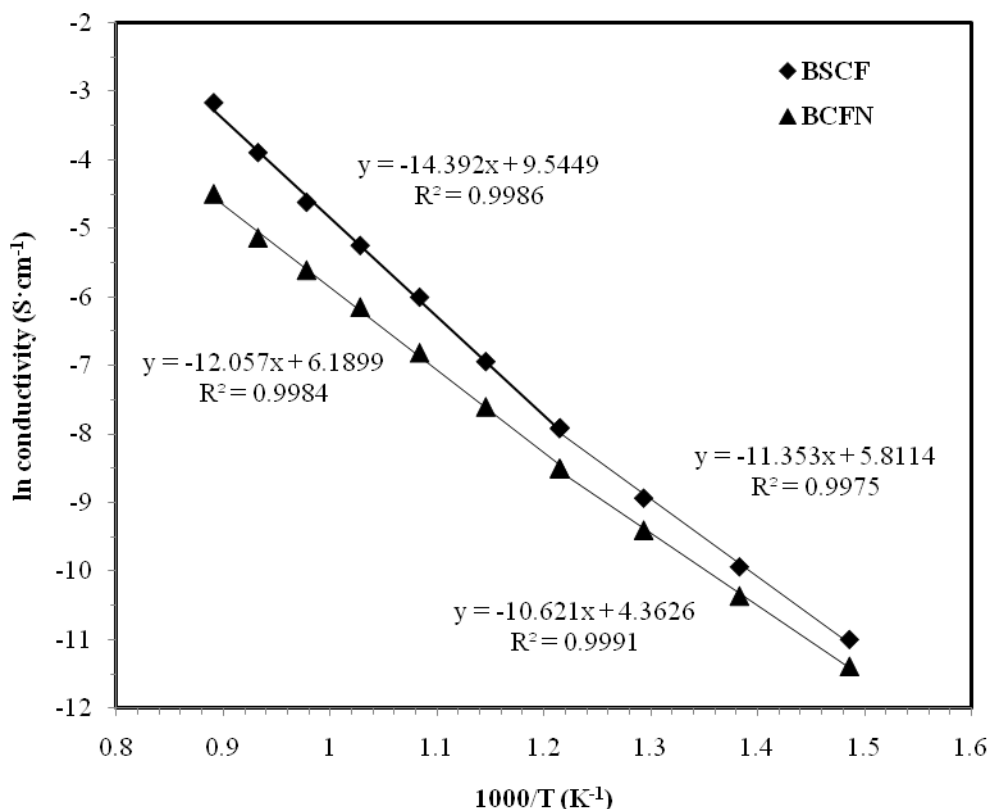


**Figure 4.6** Electrical conductivity of BSCF and BCFN at 400-850°C.

### 4.3 Oxygen permeation

#### 4.3.1 Oxygen permeation of BSCF membranes

##### 4.3.1.1 Single-coating BSCF membrane

The oxygen permeation flux of single-coated and uncoated BSCF membranes are shown in Figure 4.7 a) and b). It was found that the oxygen permeation flux increased monotonically with increasing temperature. In Figure 4.7 a), BSCF membranes were coated with LSCF, SCF and SCFN on the air side (high oxygen partial pressure side). The oxygen permeation fluxes of the membranes decreased as the following order, SCF > LSCF > no catalyst > SCFN. This could be explained that SCF has a higher oxygen sorption capacity than LSCF (~ 0.41 mmol/g for SCF and ~ 0.28 mmol/g for LSCF at 800°C) [24]; therefore, SCF could absorb oxygen atoms as the oxide ions faster than LSCF could, resulting in higher oxygen permeation flux. Therefore, the single-coating of SCF on the air side of BSCF gave a higher oxygen permeation flux than that of LSCF.

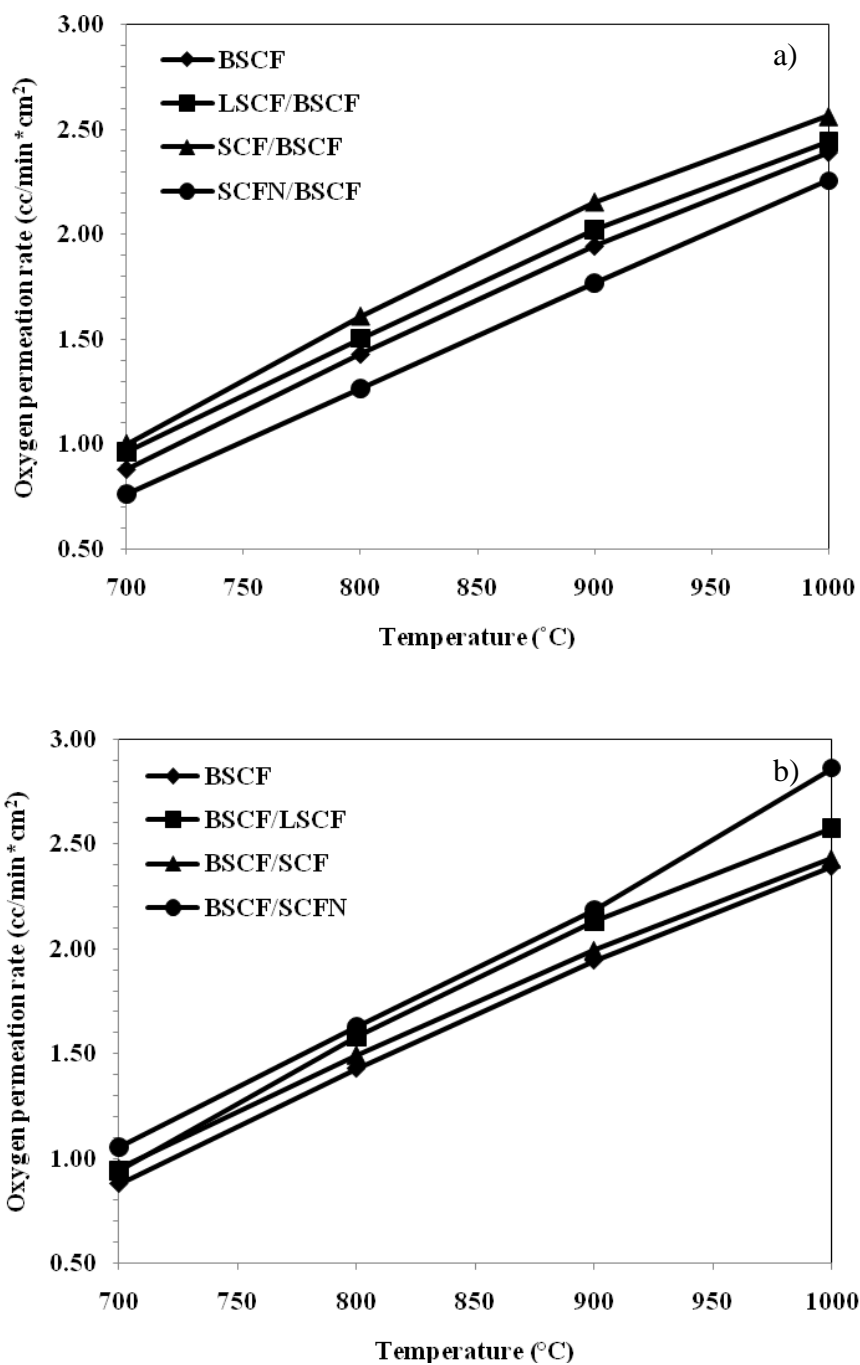


**Figure 4.7** Oxygen permeation fluxes of uncoated and coated BSCF membranes on a) the air side and b) the He side.

In Figure 4.7 b), membranes were coated by LSCF, SCF and SCFN on He side (low oxygen partial pressure side). On this side, the oxygen permeation fluxes of the membranes differed as the followings: SCFN > LSCF > SCF > no catalyst. All coated

BSCF membranes showed higher oxygen permeation fluxes than uncoated BSCF membrane. BSCF membrane coated by SCFN showed the highest oxygen permeation flux. The reason could be that  $\text{SrCo}_{0.4}\text{Fe}_{0.5}\text{Ni}_{0.1}\text{O}_3$  has a higher  $\alpha$ -oxygen desorption (about 1.43 time) than  $\text{SrCo}_{0.4}\text{Fe}_{0.6}\text{O}_3$  [28] (the main phase in SCF) because doping with low valence metal ions ( $\text{Ni}^{2+}$ ) can increase oxygen vacancy concentration leading to the increase in the amount of  $\alpha$ -oxygen desorption. As a consequence, SCFN released oxide ions as oxygen gas faster than other catalysts.

#### 4.3.1.2 Double-coating BSCF membrane

From the previous discussion, SCF was the best catalyst on the air side while SCFN and LSCF were excellence catalysts on the He side. The results led us to coat both sides of the membrane using SCF on the air side and SCFN or LSCF on the He side (SCF/BSCF/SCFN or SCF/BSCF/LSCF, respectively) as illustrated in Figures 4.8 – 4.10. Figure 4.8 showed that a double-coating of SCF on the air side and LSCF on the He side did not further increase the flux of a single-coating. While a double coating of SCF on the air side and SCFN on the He side in Figure 4.9, showed a better oxygen permeation flux than a single-coating. The effect of double-coating increased an oxygen permeation flux as compared to the flux of blank BSCF membrane. Furthermore, SCF/BSCF/SCFN double-coating system had higher oxygen permeation flux than SCF/BSCF/LSCF system, as shown in Figure 4.10, similar to the effect of single-coating on the He side by SCFN and LSCF.

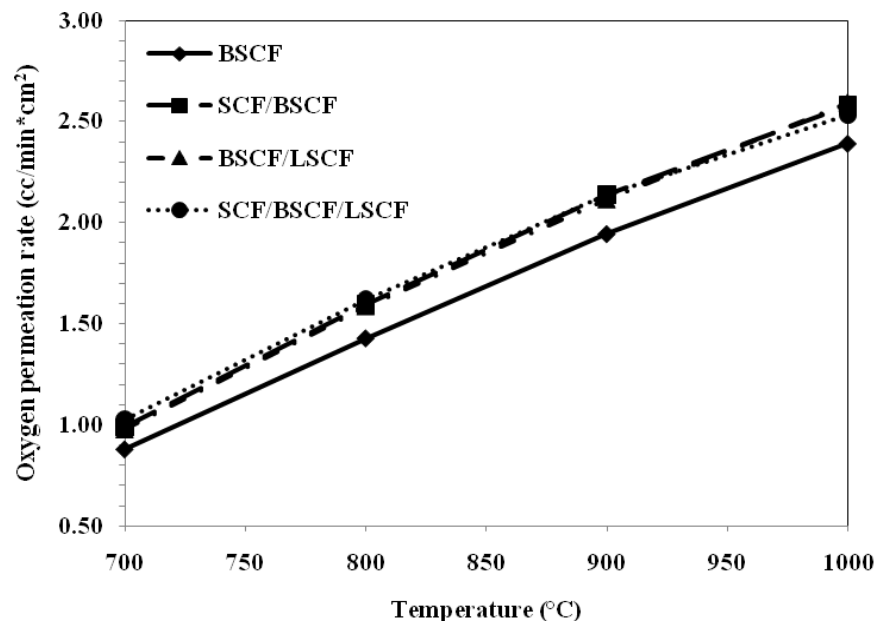


**Figure 4.8** Oxygen permeation fluxes of uncoated, single-coated and double-coated BSCF membranes by SCF on the air side and LSCF on the He side.

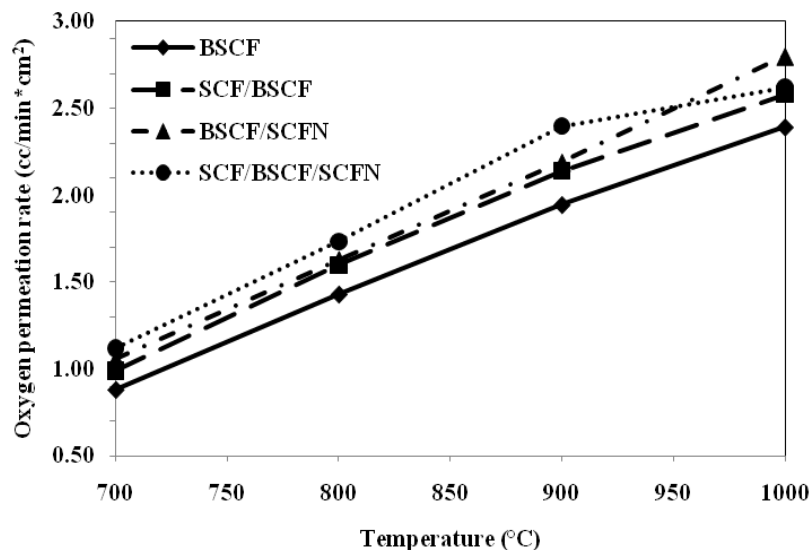


**Figure 4.9** Oxygen permeation fluxes of uncoated, single-coated and double-coated BSCF membranes by SCF on the air side and SCFN on the He side.

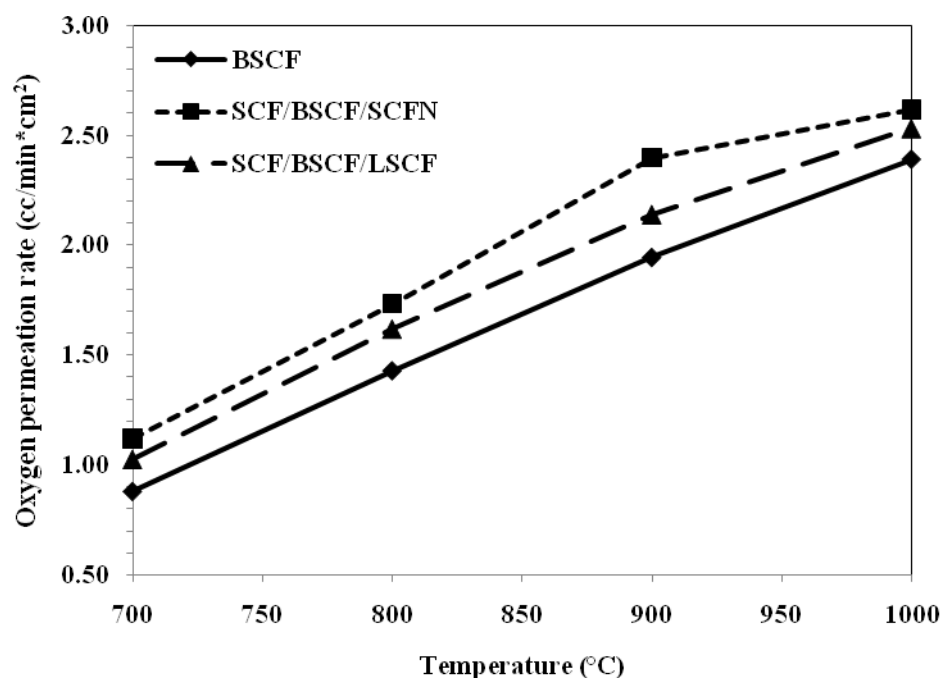


**Figure 4.10** Oxygen permeation fluxes of uncoated and double-coated BSCF membranes.

### 4.3.2 Oxygen permeation of BCFN membrane

Although the single-phased BCFN was successfully synthesized, the dense BCFN membrane could not be achieved. The best attempt resulted in the maximum relative density of BCFN membrane of 79.28% while the relative density must be higher than 90% in order to be dense enough to be used as a gas membrane. Therefore, a proper experiment on oxygen permeation was not achieved. An investigation on the preparation of BCFN membrane was described below.

The preparation of single-phased BCFN was described in section 4.1.1 using the calcination temperature of 1100°C for 20 h and the sintering temperature of 1150°C for 20h. However, a dense membrane could not be prepared from the prepared powder. Hence, the synthesized condition was varied. At first, the sintering temperature was varied. BCFN powder was prepared via solid state method. The mixture of starting materials was calcined at 900°C for 5 h, then pressed at 20 MPa into a pellet and sintered at 1100°C, 1150°C and 1200°C. The single-phased perovskite was obtained at sintering temperature of 1150°C as shown in Figure 4.11.

Furthermore, the pellet started to melt at the sintering temperature of 1200°C; therefore, the maximum sintering temperature must be 1150°C. The second variation was calcination temperature. The sintering temperature was then fixed at 1150°C and the calcination temperature was varied from 800°C – 1100°C for 5 h. The results showed that single-phased perovskite was obtained at all temperatures. The effect of calcination temperature upon a relative density was revealed in Table 4.2 showing a decrease of the relative density as the calcination temperature increased. This could be explained that normally the size of particles is larger at higher calcination temperature because a higher temperature causes faster molecular motion and rapid crystal formation [44], and the packing of larger particles created a large void space. The highest relative density of 70.87% was obtained when using the powder calcined at 800°C. In order to decrease the number of voids and increase the contact between the particles, pressing force in the process of making the pellet was varied from 20 MPa to 48 MPa and the results were tabulated in table 4.3. It was found that the maximum relative density of 75.24% was obtained when pressed at 30 MPa. When pressed at 48MPa, the membranes cracked.

The problem in making the dense membrane of BCFN could also be noticed in previous reports. Zhang *et al.* [17] prepared a dense BCFN membrane via solid state method with the calcination temperature of 1100°C for 20h and then pressed to pellet at 48 MPa, followed by sintering at 1150°C for 5 - 20h. According to that report, the relative density of the membrane reached 79.28% using the calcination temperature of 1100°C for 20h and then pressed to pellet at 48 MPa. Therefore, the investigation of BCFN membrane in this work could not be further continued.

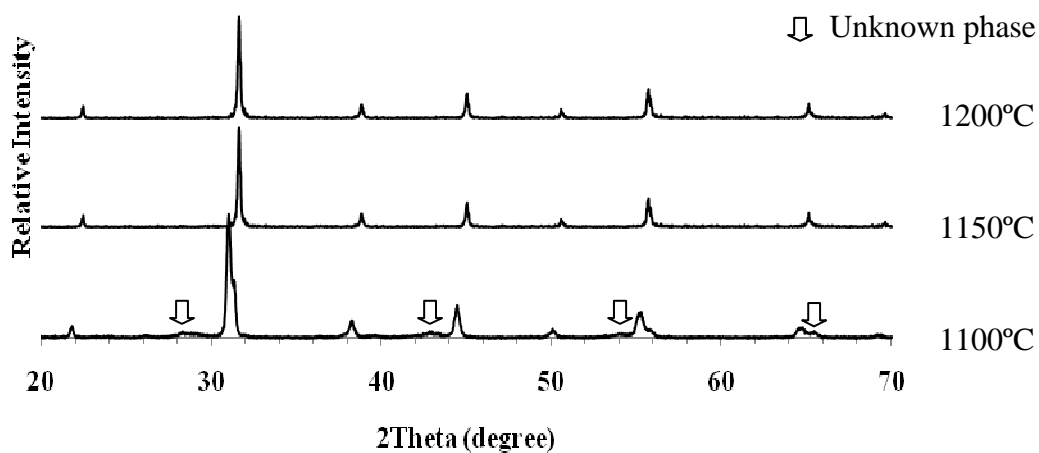


**Figure 4.11** XRD patterns of BCFN membranes at various sintering temperatures.

**Table 4.2** Relative densities of BCFN membrane prepared from the powder calcined at various temperatures

Calcination temperature (°C)	Relative density (%)
800	70.87
900	69.52
1000	64.21
1100	59.75

**Table 4.3** Relative densities of BCFN membrane prepared at different pressures

Pressure (MPa)	Relative density (%)
20	70.87
30	75.24
48 (Maximum)	crack



#### 4.4 Compatibility between membranes and catalysts

The membranes coated by catalysts need to be tested for the chemical compatibility between the membrane and catalysts. If these two components react with each other at high temperature, the new phase may reduce the conductivity between membrane and catalysts and decrease the performance of the membrane.

##### 4.4.1 Compatibility between membranes and catalysts monitored by XRD

Figures 4.12, 4.13 and 4.14 are the XRD patterns of the powder mixtures of BSCF with the catalysts LSCF, SCFN and SCF, respectively. Figure 4.12 shows that the new phase occurred when fired at 950°C for 10 h. And after firing at 1000°C for 10 h, BSCF peaks and LSCF peaks disappeared and the strong peak of a new phase which has a structure similar to  $(\text{La}_{0.3}\text{Sr}_{0.7})\text{FeO}_3$  (JCPDS: 82-1964) was formed. Therefore, BSCF has a good compatibility with LSCF below 950°C. While the XRD patterns of mixed BSCF and SCFN powders in Figure 4.13 show that the new phases occurred when fired at 900°C for 10 h. After firing at 1000°C for 10 h, BSCF peak and LSCF peak slightly disappeared and showed several strong peaks of new phases which were identified as  $\text{SrFeO}_{3-x}$  and  $\text{BaFe}_2\text{O}_4$  (JCPDS: 34-0641 and JCPDS: 26-0721, respectively). Therefore, BSCF has a good compatibility with SCFN below 900°C. In the case of SCF catalyst, the XRD patterns of mixed BSCF and SCF powders on Figure 4.14 show that the new phases occurred when fired at 900°C for 10 h. After firing at 1000°C for 10 h, BSCF peaks and SCF peaks disappeared and showed strong new phases which could be identified as  $\text{SrCoO}_{2.29}$  and  $\text{CoO}$  (JCPDS: 39-1083 and JCPDS: 481719, respectively). Therefore, BSCF has a good compatibility with SCF below 900°C.

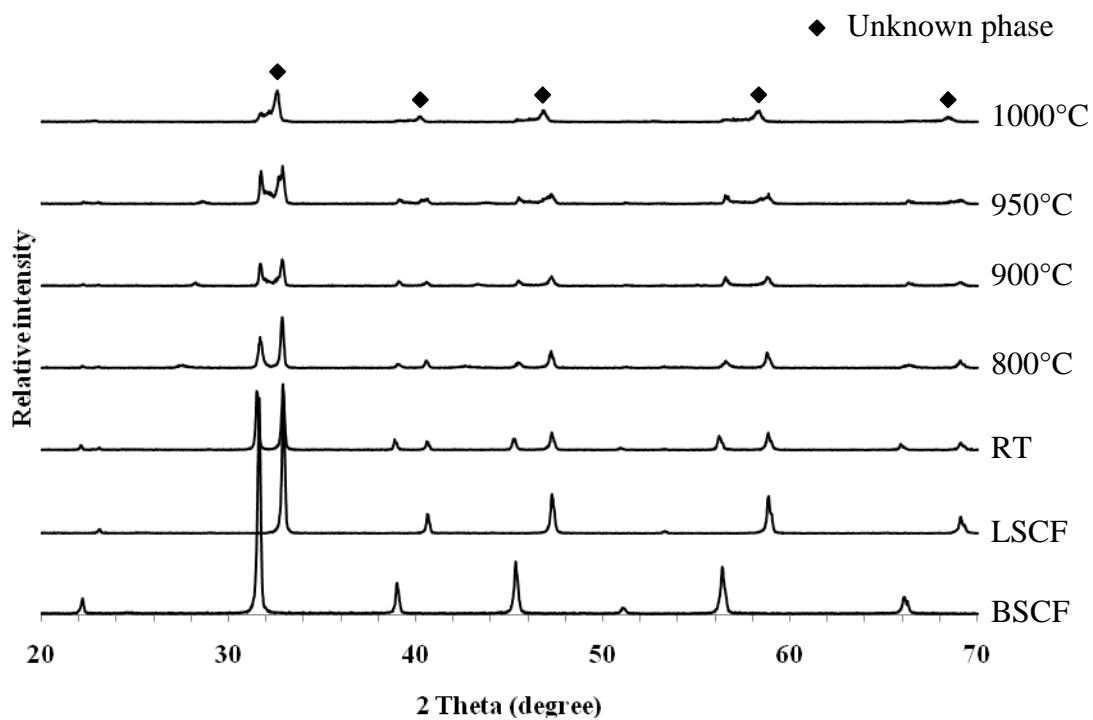


**Figure 4.12** XRD patterns of the mixture of BSCF and LSCF powders firing from 800°C to 1000°C in the period of 10 h for each temperature.

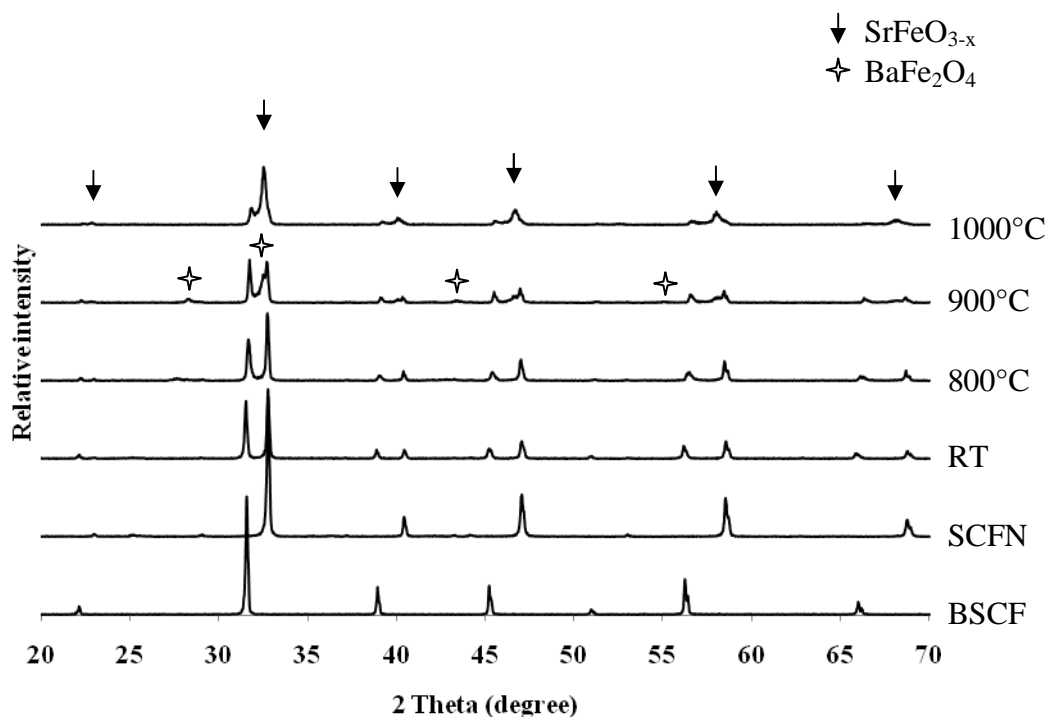


**Figure 4.13** XRD patterns of the mixture of BSCF and SCFN powders firing from 800°C to 1000°C in the period of 10 h for each temperature.

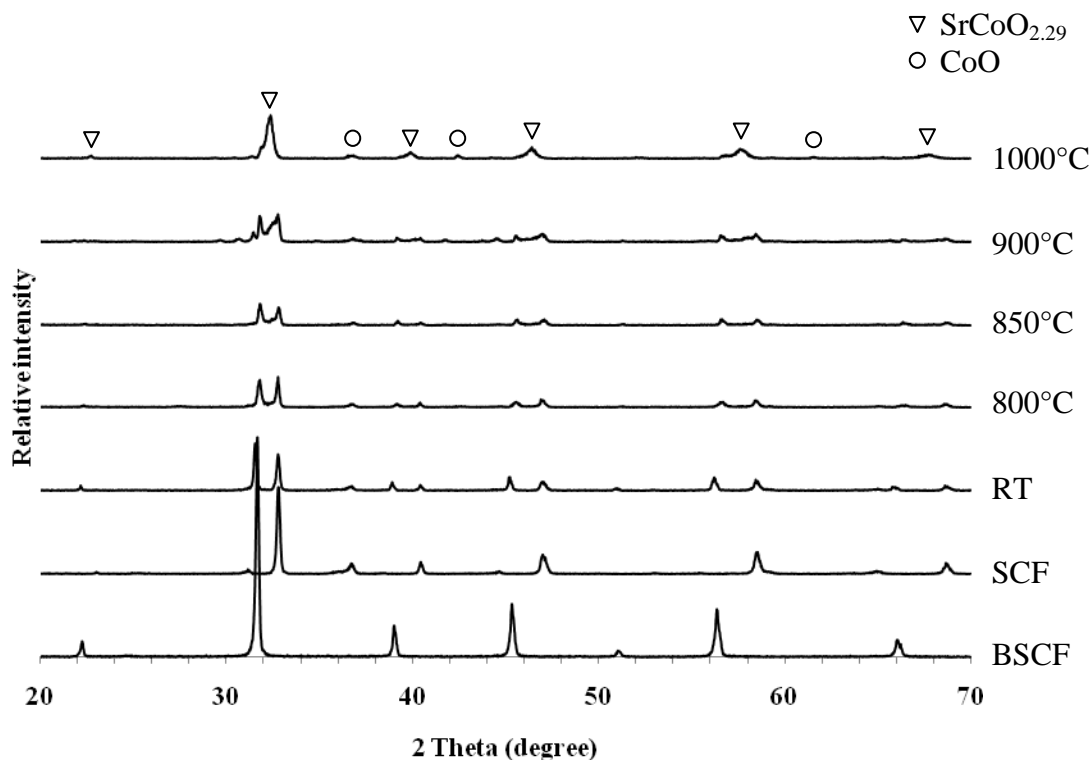


**Figure 4.14** XRD patterns of the mixture of BSCF and SCF powders firing from 800°C to 1000°C in the period of 10 h for each temperature.

#### 4.4.2 Compatibility between membranes and catalysts monitored by SEM/EDS

##### 4.4.2.1 Surface of coated and uncoated membranes

Figures 4.15-18 are the SEM images of the surface of coated and uncoated BSCF membranes. For the uncoated BSCF membrane in Figure 4.15, the results show that lots of small pores appeared on both sides of BSCF surface after being tested for the oxygen permeation in the temperature range of 700 – 1000°C. It could be explained that the stream of high pressure oxygen gas adsorbed on the surface and in the pores of the surface on the air side could create small pores after a period of time. The morphology of the surface on the He side was changed dramatically and small pores appeared over the whole surface which could be the result of fast desorption from solid membrane. The EDS result, Figure 4.15 d), shows that an amount of A-side cations which are Ba and Sr increased at the surface while

the amount of B-site cations which are Co and Fe decreased on the surface. It is likely that  $\text{Ba}^{2+}$  and  $\text{Sr}^{2+}$  could migrate from the bulk towards the surface as reported by Ge *et al.* in the case of  $\text{Ba}_{0.5}\text{Sr}_{0.5}\text{Co}_{0.8}\text{Fe}_{0.2}\text{O}_{3-\delta}$  [45]. Therefore, the BSCF membrane is not stable for the oxygen permeation test at  $1000^\circ\text{C}$ .

For the coated BSCF membranes, as shown in Figures 4.16-18, the catalysts coated on BSCF were fine particles which have high surface area and the coating was also loosely-packed. Therefore, the morphologies of catalysts for both the air side and the He side were not changed after being used in the oxygen permeation tests because the high porosities possessed enough surface area for the oxygen exchange reaction. The EDS results of coated BSCF membrane; Figures 4.16 d), 4.17 d) and 4.18 d), showed that the amounts of all metals were not significantly changed after being used in the oxygen permeation tests, except those of BSCF membranes coated with LSCF on the air side and with SCFN on the He side. According to the results from section 4.4.1, the mixture of BSCF and catalyst powder showed new phases after heating at  $1000^\circ\text{C}$ . The formation of new phases resulted to the change in the amounts of metal on the surface.

Although the morphologies of the catalysts that coated on both surfaces of BSCF membrane were not changed after testing for oxygen permeation at  $1000^\circ\text{C}$ , the phases and compositions of some catalysts, such as SCFN, were changed. Therefore, the metal amounts of the cross section of coated BSCF membranes after being tested for oxygen permeation at  $1000^\circ\text{C}$  were also measured.

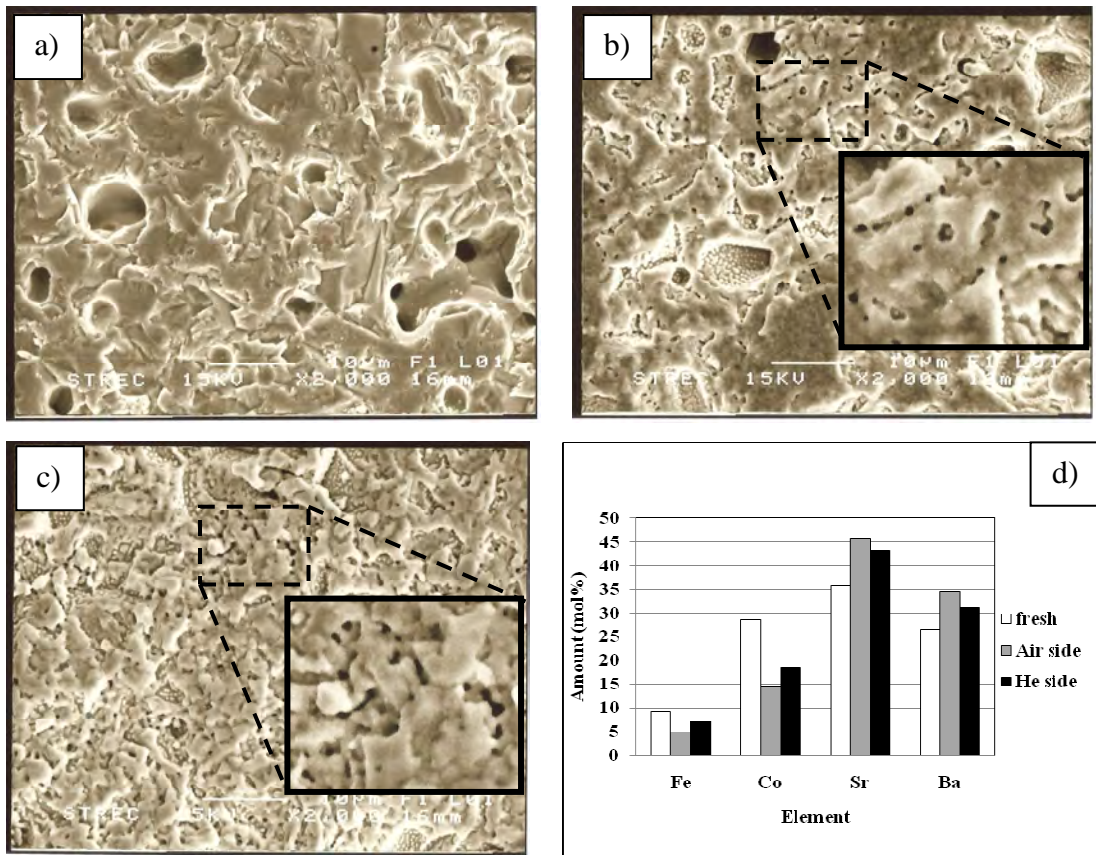


**Figure 4.15** SEM images of the surface of BSCF membrane before and after being tested for oxygen permeation; a) before, b) air side, c) He side and d) the EDS analysis of a) – c).

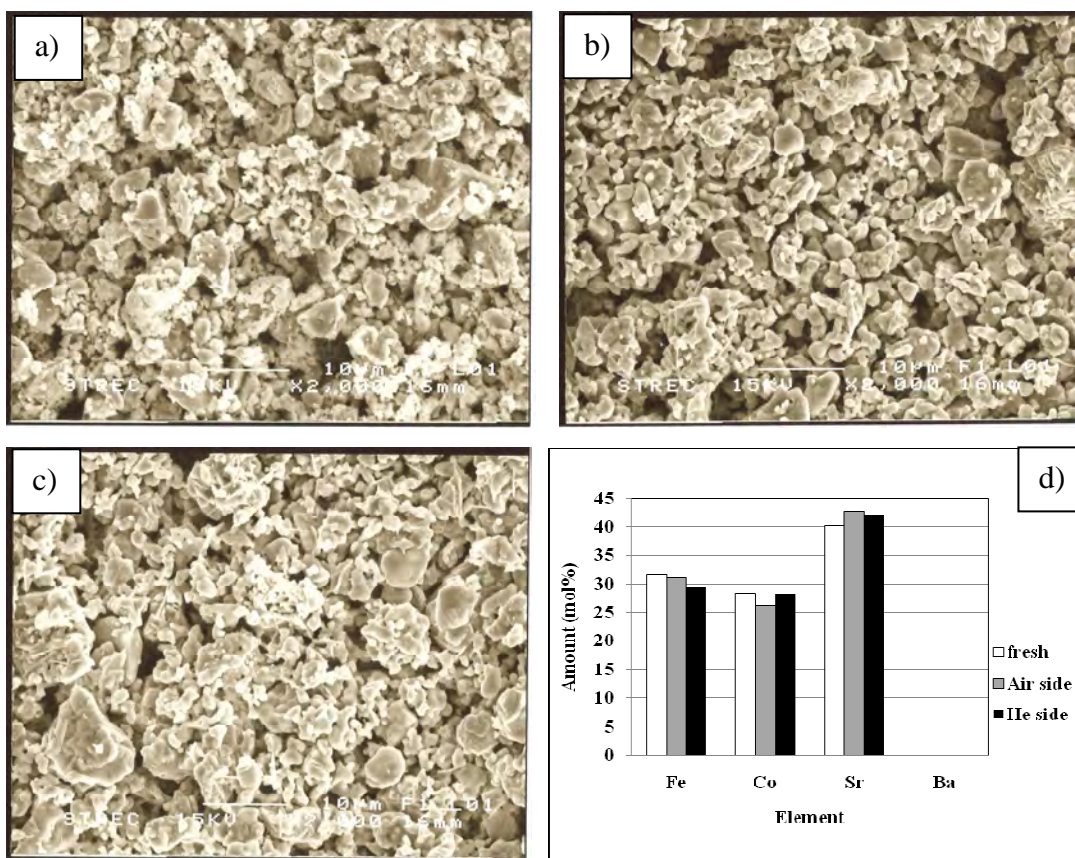


**Figure 4.16** SEM images of the surface of BSCF membrane coated by SCF before and after being tested for oxygen permeation; a) before, b) air side, c) He side and d) the EDS analysis of a) – c).

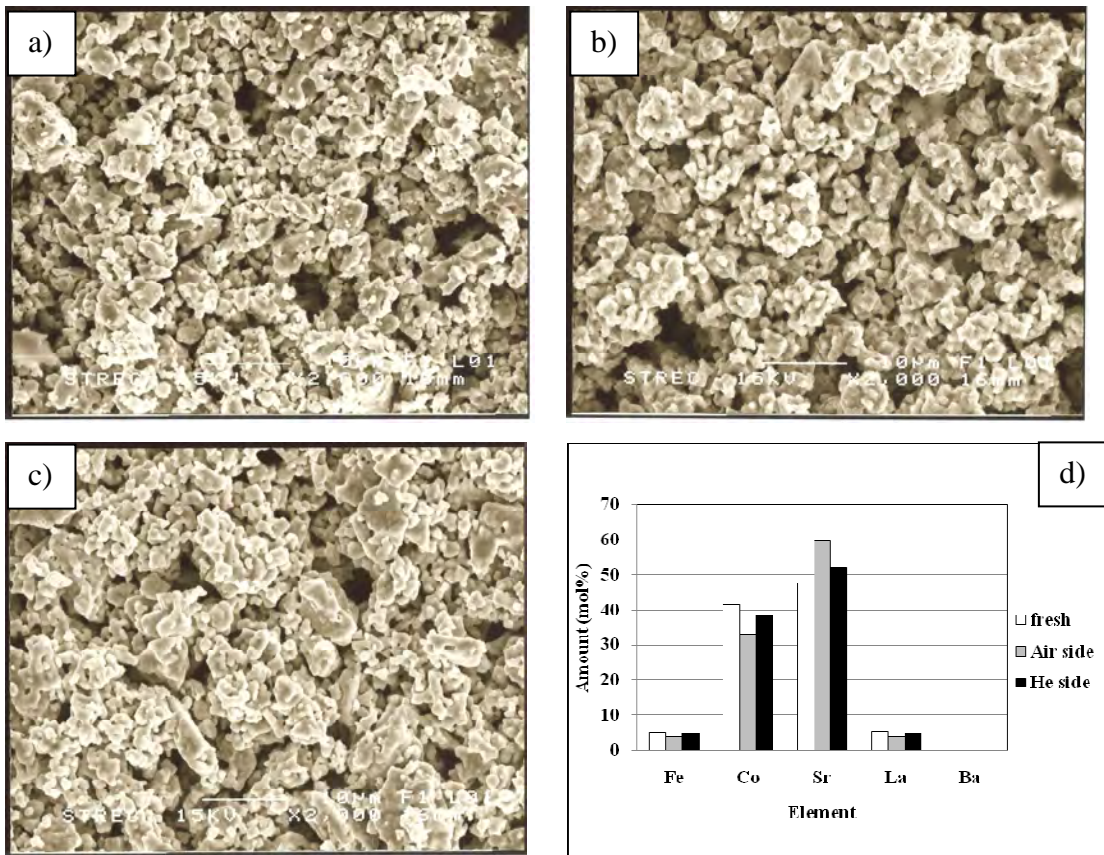


**Figure 4.17** SEM images of the surface of BSCF membrane coated by LSCF before and after being tested for oxygen permeation; a) before, b) air side, c) He side and d) the EDS analysis of a) – c).



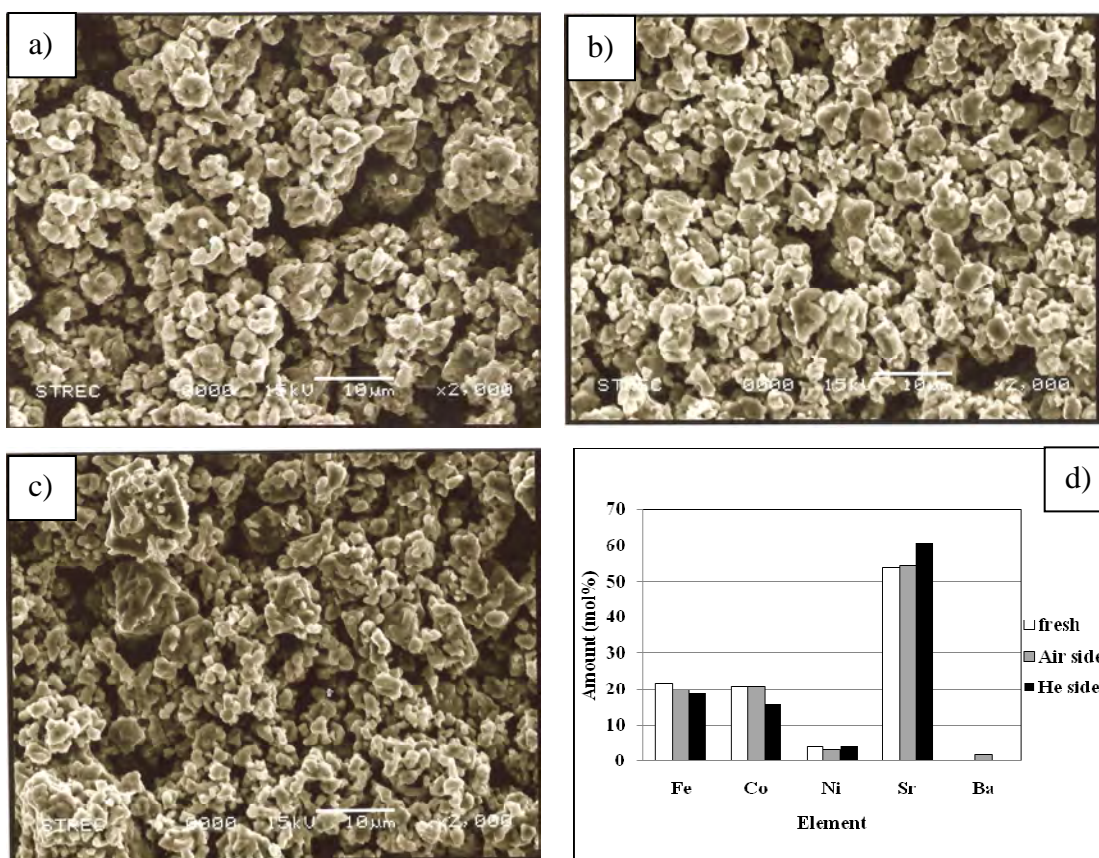


**Figure 4.18** SEM images of the surface of BSCF membrane coated by SCFN before and after being tested for oxygen permeation; a) before, b) air side, c) He side and d) the EDS analysis of a) – c).

#### 4.4.2.2 Cross section of coated and uncoated membranes

The chemical compatibility of BSCF membrane and catalysts was monitored by SEM/EDS. Figures 4.19 – 4.24 are SEM images of the cross section of BSCF membranes coated by SCF, LSCF and SCFN catalysts before and after being used in the oxygen permeation tests. The diffusion of metal ions from catalyst coating to BSCF membrane and vice versa after use was investigated. Two points on the cross-section image were chosen. The first point (1) is on the BSCF membrane. Ideally, only Ba, Sr, Co and Fe ions would be detected at (1) if there is no reaction between the two phases. Likewise, only the metals comprised in each catalyst would be found at the second point (2) in the catalysts region. However most metal elements

appear in both BSCF and catalysts such as Sr, Co, and Fe, the changes of an amount for each element must be considered as well.

Figures 4.19 and 4.20 showed BSCF membrane coated with SCF on the air side and the He side, respectively. The results from both cases show that the amounts of Sr and Co of SCF catalyst layer decreased while the amount of Fe increased. Moreover, the diffusion of Ba from the BSCF membrane into the SCF catalyst was observed. According to section 4.4.1, the new phases of  $\text{SrCoO}_{2.29}$  and CoO were found after heating at  $1000^\circ\text{C}$ , so it might be that Sr and Co migrated from SCF catalyst to form the impurity phases of  $\text{SrCoO}_{2.29}$  and CoO in the membrane region.

Figures 4.21 and 4.22 showed BSCF membrane coated with LSCF on the air side and the He side respectively. The results from both cases show that the amounts of Fe, Co and La of LSCF catalyst layer decreased while the amount of Sr increased. Moreover, the diffusion of Ba from the BSCF membrane into the SCF catalyst was observed. According to section 4.4.1, the new phase of  $(\text{La}_{0.3}\text{Sr}_{0.7})\text{FeO}_3$  was formed after heating at  $1000^\circ\text{C}$  that could lead to the change in the composition nearby the interface. However, the differences of the metal compositions between fresh and used coating membranes were much smaller compared to the change in BSCF/SCF membrane.

Figures 4.23 and 4.24 showed BSCF membrane coated with SCFN on the air side and the He side, respectively. The results show that a little amount of Ba diffused from the BSCF membrane into the SCFN catalyst while a trace of Ni diffused from SCFN catalyst into BSCF membrane for both sides.

From all cases, it was found that Ba diffused from BSCF membrane into the catalysts. However, the diffusion of Ba was so little that no other compound of barium could be detected by XRD.

All coated membranes were tested for oxygen permeation at  $1000^\circ\text{C}$  before analysis by SEM/EDS; therefore, according to these results, these coated BSCF membranes could not be used at  $1000^\circ\text{C}$ . The chemical compatibility monitored by XRD in section 4.4.1 showed the maximum temperatures for coated BSCF membranes that are under  $900^\circ\text{C}$  for the membrane coated with SCF or SCFN and under  $950^\circ\text{C}$  for the membrane coated with LSCF.

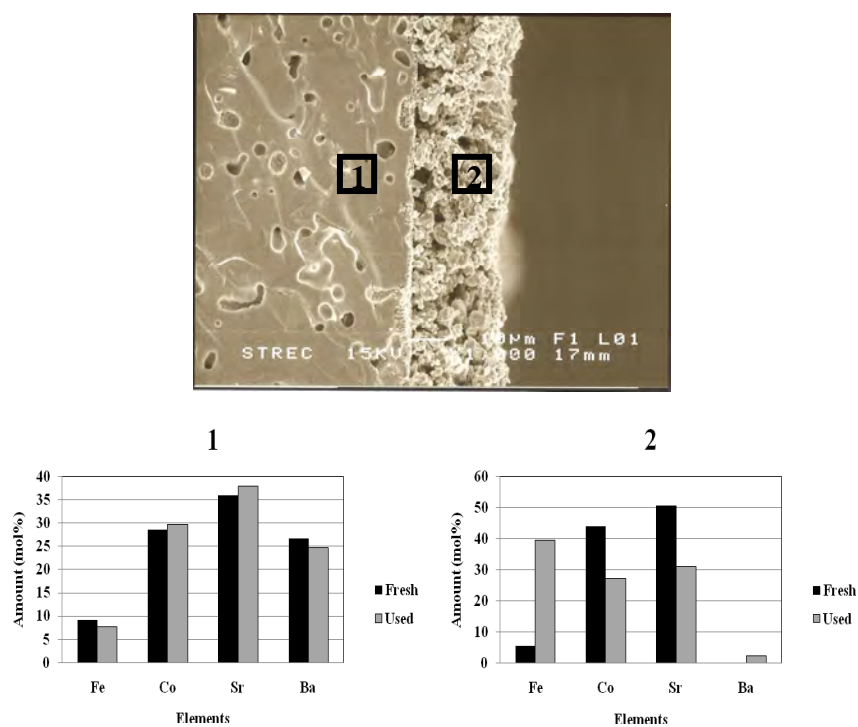


**Figure 4.19** SEM images of the cross section of BSCF membrane coated with SCF on the air side before and after being tested for oxygen permeation.

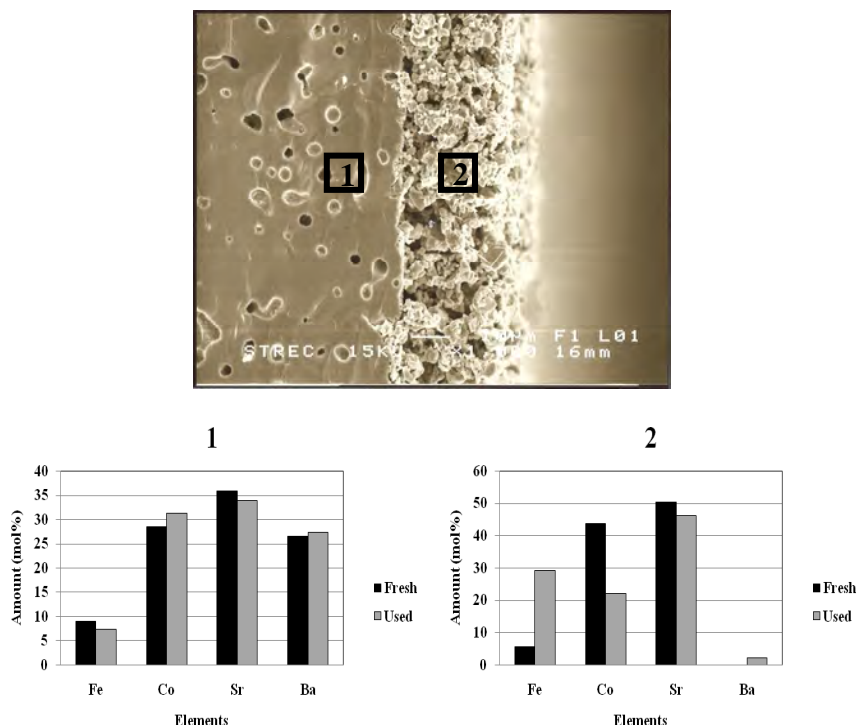


**Figure 4.20** SEM images of the cross section of BSCF membrane coated with SCF on the He side before and after being tested for oxygen permeation.

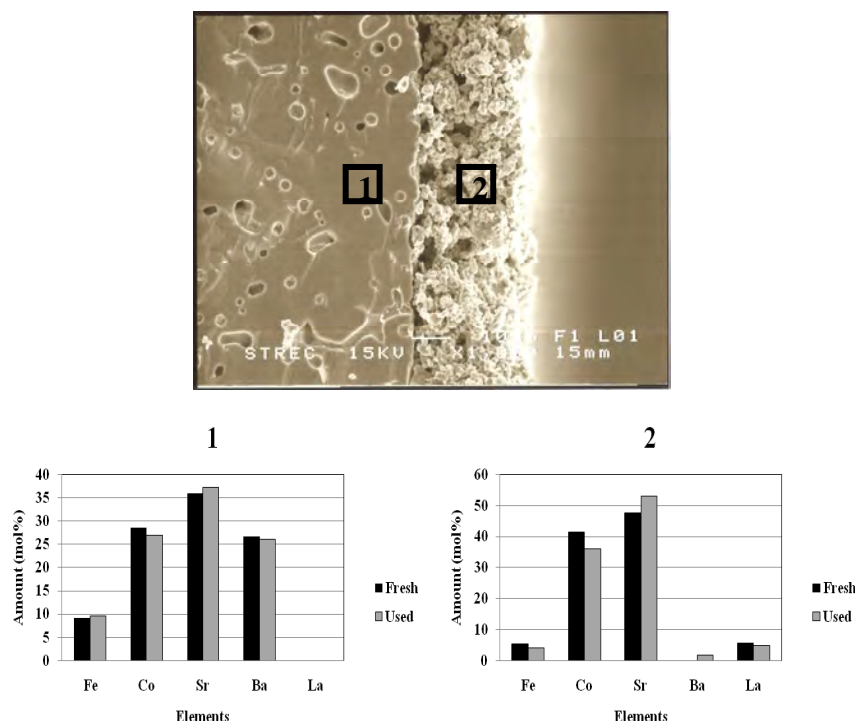


**Figure 4.21** SEM images of the cross section of BSCF membrane coated with LSCF on the air side before and after being tested for oxygen permeation.

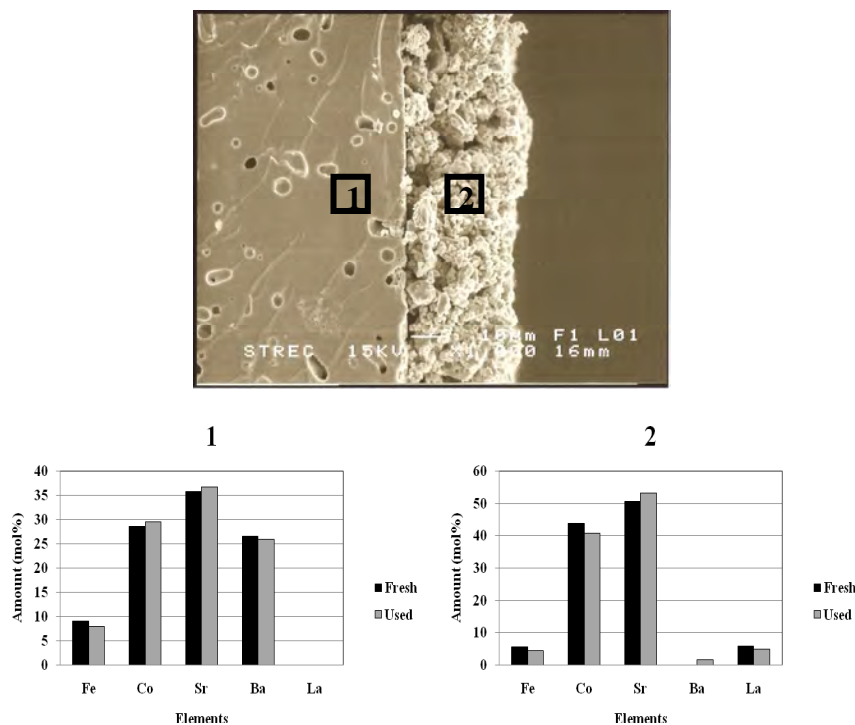


**Figure 4.22** SEM images of the cross section of BSCF membrane coated with LSCF on the He side before and after being tested for oxygen permeation.

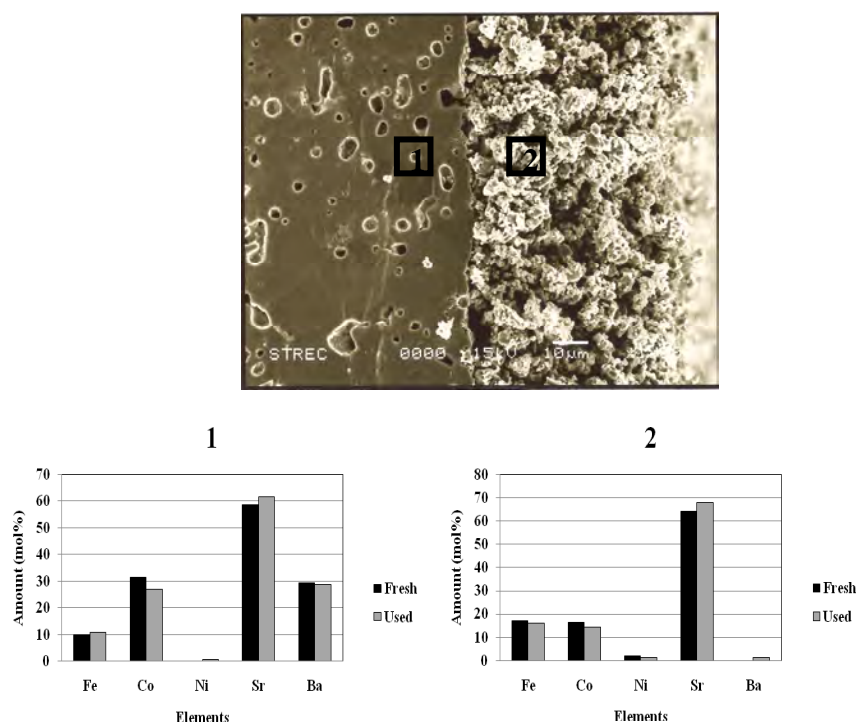


**Figure 4.23** SEM images of the cross section of BSCF membrane coated with SCFN on the air side before and after being tested for oxygen permeation.

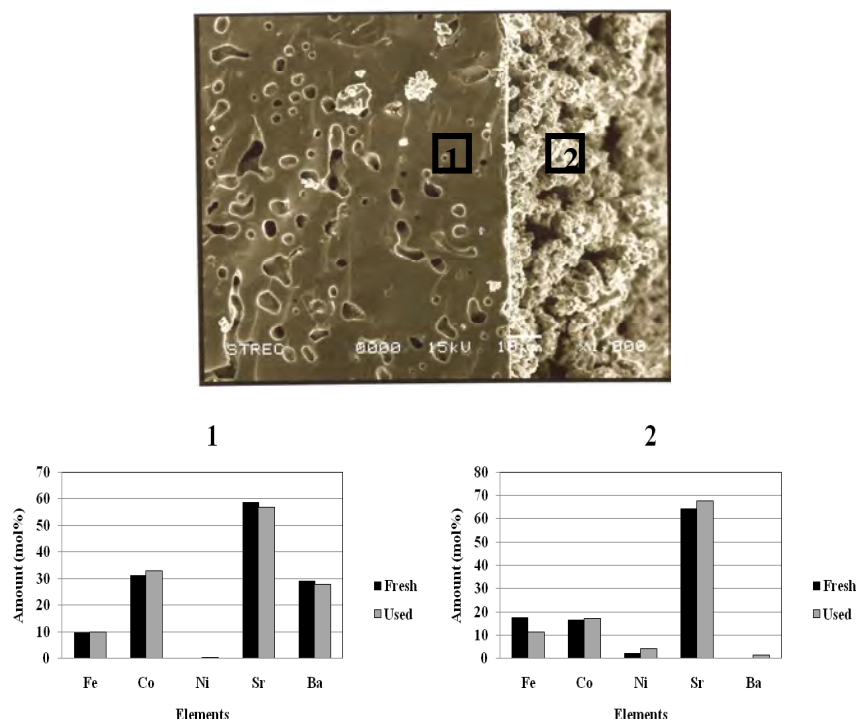


**Figure 4.24** SEM images of the cross section of BSCF membrane coated with SCFN on the He side before and after being tested for oxygen permeation.

#### 4.5 Long-term stability

For a practical application of catalyst-coating membrane, not only high oxygen permeation flux is required, a good stability of oxygen permeation over a long-term is also of importance. According to Lu *et al.* [46], BSCF membrane has a good oxygen permeation stability at 850°C and the compatibility between membranes and catalysts from section 4.4 exhibited a good compatibility of BSCF membrane with SCF and SCFN at 850°C. Therefore, this experiment investigated the long-term stability of BSCF membrane coated with SCF on the air side and SCFN on the He side at 850°C. The result (Figure 4.25), showed that the membrane has a good oxygen permeation stability at 850°C for at least 100h.

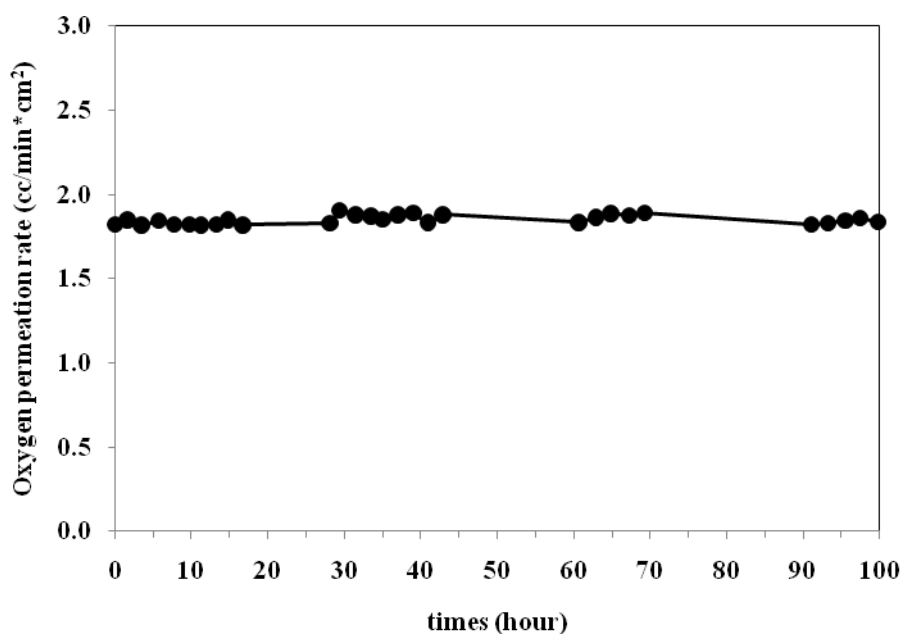


**Figure 4.25** The long-term stability of BSCF membrane that was coated with SCF on the air side and SCFN on the He side at 850°C.

# **CHAPTER V**

## **CONCLUSIONS AND SUGGESTION**

### **5.1 Conclusions**

#### **Synthesis of materials**

Single-phased BSCF was successfully synthesized via the solid state method with the calcination temperature of 900°C for 5 h and the sintered temperature of 1200°C. Similarly, single-phased BCFN was synthesized via the solid state method with the calcination temperature of 1100°C for 10 h and the sintered temperature of 1150°C. Both BSCF and BCFN have high electrical conductivities, but the relative density of BCFN membrane is too low to use as a dense ceramic membrane for gas permeation reactor. Therefore, only BSCF membrane was studied for the oxygen permeation property. For the catalyst materials, SCF, LSCF and SCFN were synthesized via the modified citrate method with the calcination temperature of 900°C, 950°C and 950°C for 5 h respectively.

#### **Oxygen permeation**

The oxygen permeation flux of the membranes was measured in the temperature range of 700 – 1000°C. The oxygen permeation fluxes of all coated membranes were higher than that of the uncoated BSCF membrane except the coating of SCFN on the air side. Comparing the effect of single-coating on the air side, coating of SCF showed higher flux than coating with LSCF and SCFN. On the other hand, comparing the effect on the He side, coating with SCFN gave higher flux than LSCF and SCF. Furthermore, a double coating with SCF on the air side and SCFN on the He side increased the flux of a single-coating.

#### **Chemical compatibility of BSCF membrane with catalysts**

The compatibility of BSCF membrane and catalysts was monitored by XRD and SEM/EDS. BSCF membrane has good chemical compatibility with SCF, LSCF and SCFN at 850°C, 900°C and 850°C, respectively.

### **Long-term stability**

The BSCF membrane coated with SCF on the air side and SCFN on the He side has good stability in the reactor at 850°C for at least 100 h.

The BSCF membrane coated by SCF on the air side and SCFN on the He side has improved oxygen permeation flux as compared to the flux of uncoated BSCF membrane, and that coated BSCF membrane is also stable at the operating temperature of 850°C for 100 h. Therefore this coated BSCF membrane could be a good candidate as a membrane for oxygen separation from air at 850°C.

### **5.2 Suggestion**

In order to apply the BSCF membrane coated by SCF on the air side and SCFN on the He side as the candidates for oxygen separation for SOFC, the optimum flow rate of air and He must be investigated.



## REFERENCES

- [1] “Oxygen for the Steel Industry” [online]. 2011. Available from:  
<http://www.praxair.com/praxair.nsf/AllContent/7DE475C5D217B2D68525706525706F00191545?OpenDocument&URLMenuBranch=764D93B15762A5538525706F00243615> [2011, April 18].
- [2] “Oxygen Plant Application” [online]. 2011. Available from: <http://www.gas-plants.com/oxygen-plant-application.html> [2011, April 18].
- [3] Leo, A., Liu, S.M. and Diniz da Costa, J.C. Development of mixed conducting membranes for clean coal energy delivery. *Int. J. Greenh. Gas Con.* 3 (2009) 357–67.
- [4] Hashim, S.S., Mohamed, A.R. and Bhatia, S. Oxygen separation from air using ceramic-based membrane technology for sustainable fuel production and power generation. *Renew. Sust. Energ. Rev.* 15 (2011): 1284–1293.
- [5] Sunarso, J. et al. Mixed ionic–electronic conducting (MIEC) ceramic-based membranes for oxygen separation. *J. Membr. Sci.* 300 (2008): 13–41.
- [6] Liu, L.M. et al. A thermo – gravimetric study of the phase diagram of strontium cobalt iron oxide,  $\text{SrCo}_{0.8}\text{Fe}_{0.2}\text{O}_{3-\delta}$ . *Mater. Res. Bull.* 31 (1996): 29 – 35.
- [7] Qiu, L., Lee, T.H., Liu, L.M., Yang, Y.L. and Jacobson, A.J. Oxygen permeation studies of  $\text{SrCo}_{0.8}\text{Fe}_{0.2}\text{O}_{3-\delta}$ . *Solid State Ionics* 76 (1995): 321 – 329.
- [8] Pei, S., Kleefisch, M.S., Kobylinski, T.P., Faber, J. and Udovich, C.A. Failure mechanisms of ceramic membrane reactors in partial oxidation of methane to synthesis gas. *Catal. Lett.* 30 (1995): 201 – 212.
- [9] Shao, Z. et al. Investigation of the permeation behavior and stability of a  $\text{Ba}_{0.5}\text{Sr}_{0.5}\text{Co}_{0.8}\text{Fe}_{0.2}\text{O}_{3-d}$  oxygen membrane. *J. Membr. Sci.* 172 (2000): 177 – 188.

- [10] Wang, H., Tablet, C., Feldhoff, A. and Caro, J. Investigation of phase structure, sintering, and permeability of perovskite-type  $\text{Ba}_{0.5}\text{Sr}_{0.5}\text{Co}_{0.8}\text{Fe}_{0.2}\text{O}_{3-\delta}$  membranes. *J. Membr. Sci.* 262 (2005): 20 – 26.
- [11] Wang, H., Tablet, C., Feldhoff, A., and Caro, J. Investigation of phase structure, sintering, and permeability of perovskite-type  $\text{Ba}_{0.5}\text{Sr}_{0.5}\text{Co}_{0.8}\text{Fe}_{0.2}\text{O}_{3-\delta}$  membranes. *J. Membr. Sci.* 262 (2005): 20 – 26.
- [12] McIntosh, S., Vente, J. F. and Haije, W.G. Structure and oxygen stoichiometry of  $\text{SrCo}_{0.8}\text{Fe}_{0.2}\text{O}_{3-\delta}$  and  $\text{Ba}_{0.5}\text{Sr}_{0.5}\text{Co}_{0.8}\text{Fe}_{0.2}\text{O}_{3-\delta}$ . *Solid State Ionics* 177 (2006): 1737 – 1742.
- [13] Liu, B. and Zhang, Y.  $\text{Ba}_{0.5}\text{Sr}_{0.5}\text{Co}_{0.8}\text{Fe}_{0.2}\text{O}_3$  nanopowders prepared by glycine–nitrate process for solid oxide fuel cell cathode. *J. Alloy. Compd.* 453 (2008): 418 – 422.
- [14] Bo, Y., Wenqiang, Z., Jingming, X. and Jing, C. Microstructural characterization and electrochemical properties of  $\text{Ba}_{0.5}\text{Sr}_{0.5}\text{Co}_{0.8}\text{Fe}_{0.2}\text{O}_{3-\delta}$  and its application for anode of SOEC. *Int. J. Hydrogen Energ.* 33 (2008): 6873 – 6877.
- [15] Zeng, P. et al. Re-evaluation of  $\text{Ba}_{0.5}\text{Sr}_{0.5}\text{Co}_{0.8}\text{Fe}_{0.2}\text{O}_{3-\delta}$  perovskite as oxygen semi-permeable membrane. *J. Membr. Sci.* 291 (2007): 148 – 156.
- [16] Baumann, S. et al. Influence of sintering conditions on microstructure and oxygen permeation of  $\text{Ba}_{0.5}\text{Sr}_{0.5}\text{Co}_{0.8}\text{Fe}_{0.2}\text{O}_{3-\delta}$  (BSCF) oxygen transport membranes. *J. Membr. Sci.* 359 (2010): 102 – 109.
- [17] Zhang, Y. Et al. Total conductivity, oxygen permeability and stability of perovskite-type oxide  $\text{BaCo}_{0.7}\text{Fe}_{0.2}\text{Nb}_{0.1}\text{O}_3$  *RARE METALS* 28 (2009): 202 – 208.
- [18] Cheng, Y. et al. Investigation of Ba fully occupied A-site  $\text{BaCo}_{0.7}\text{Fe}_{0.3-x}\text{Nb}_x\text{O}_{3-\delta}$  perovskite stabilized by low concentration of Nb for oxygen permeation membrane. *J. Membr. Sci.* 322 (2008): 484 – 490.

- [19] Zhang, Y. et al. Hydrogen amplification of coke oven gas by reforming of methane in a ceramic membrane reactor. *Int. J. Hydrogen Energ.* 33 (2008): 3311 – 3319.
- [20] Zhu, C. et al. Novel  $\text{BaCo}_{0.7}\text{Fe}_{0.3-y}\text{Nb}_y\text{O}_{3-d}$  ( $y = 0-0.12$ ) as a cathode for intermediate temperature solid oxide fuel cell. *Electrochem. Commun.* 11 (2009): 958 – 961.
- [21] Zhang, Y., Liu, J., Liu, Y., Ding, W. and Lu, X. Perovskite-type oxygen-permeable membrane  $\text{BaCo}_{0.7}\text{Fe}_{0.2}\text{Nb}_{0.1}\text{O}_3$  for partial oxidation of methane in coke oven gas to hydrogen. *RARE METALS* 29 (2010): 231 – 237.
- [22] Cheng, H., Zhang, Y., Lu, X., Ding, W. and Li, Q. Hydrogen Production from Simulated Hot Coke Oven Gas by Using Oxygen-Permeable Ceramics. *Energ. Fuel.* 23 (2009): 414 – 421.
- [23] Ma, B. and Balachandran, U. Phase stability of  $\text{SrFeCo}_{0.5}\text{O}_x$  in reducing environments. *Mater. Res. Bull.* 33 (1998): 223 – 236.
- [24] Yin, Q., Kniep, J. and Lin, Y.S. Oxygen sorption and desorption properties of Sr–Co–Fe oxide. *Chem. Eng. Sci.* 63 (2008): 2211 – 2218.
- [25] Kim, S., Yang, Y.L., Christoffersen, R. and Jacobson, A.J. Determination of oxygen permeation kinetics in a ceramic membrane based on the composition  $\text{SrFeCo}_{0.5}\text{O}_{3.25-d}$  *Solid State Ionics* 109 (1998): 187 – 196.
- [26] Yang, Z.H. and Lin, Y.S. High – temperature oxygen sorption in a fixed bed packed with perovskite typed ceramic sorbents. *Ind. Eng. Chem. Res.* 42 (2003): 4376 – 4381.
- [27] Kusaba, H., Shibata, Y., Sasaki, K. and Teraoka, Y. Surface effect on oxygen permeation through dense membrane of mixed conductive LSCF perovskite type oxide. *Solid state Ionics* 177 (2006): 2249 – 2253.
- [28] He, Y.J. et al. Effect of dopant oxygen desorption and oxygen permeability of  $\text{SrCo}_{0.4}\text{Fe}_{0.5}\text{M}_{0.1}\text{O}_{3-\delta}$  ( $\text{M} = \text{Ni}, \text{Al}$  and  $\text{Zr}$ ) mixed conducting oxides. *Chinese Chem. Lett.* 19 (2008): 725 – 729.

- [29] Wang, Y., Hao, H., Jia, J., Yang, D. and Hu, X. Improving the oxygen permeability of  $\text{Ba}_{0.5}\text{Sr}_{0.5}\text{Co}_{0.8}\text{Fe}_{0.2}\text{O}_{3-\delta}$  membranes by a surface-coating layer of  $\text{GdBaCo}_2\text{O}_{5+\delta}$ . *J. Eur. Ceram. Soc.* 28 (2008): 3125 – 3130.
- [30] Shen, Z., Lu, P., Yan, G. and Hu, X. Enhancing the oxygen permeability of  $\text{Ba}_{0.5}\text{Sr}_{0.5}\text{Co}_{0.8}\text{Fe}_{0.2}\text{O}_{3-\delta}$  membrane by coating  $\text{RBaCo}_2\text{O}_{5+\delta}$  (R = Pr, Nd, Sm and Gd) layers. *Mater. Lett.* 64 (2010): 980 – 982.
- [31] Lee, K.S., Lee, S., Kim, J.W. and Woo, S.K. Enhancement of oxygen permeation by  $\text{La}_{0.6}\text{Sr}_{0.4}\text{CoO}_{3-\delta}$  coating in  $\text{La}_{0.7}\text{Sr}_{0.3}\text{Ga}_{0.6}\text{Fe}_{0.4}\text{O}_{3-\delta}$  membrane. *Desalination* 147 (2002): 439 – 444.
- [32] Sammells, T. “Mixed membrane reactors for spontaneous synthesis gas production” [online]. 1999. Available from:  
<http://academic.sun.ac.za/UNESCO/Conferences/Conferences1999/Lectures1999/Sammells99/Sampresent?PRESENT.html> [1999, March 31].
- [33] “Simple drawing of perovskite structure” [online]. 2011. Available from:  
[http://www.mne.eng.psu.ac.th/staff/lek\\_files/ceramic/u1-7.htm](http://www.mne.eng.psu.ac.th/staff/lek_files/ceramic/u1-7.htm) 9/3/54 [2011, March 9].
- [34] West, A.R. *Basic solid state chemistry*, 2<sup>nd</sup> ed., Wiley, Singapore, 1999.
- [35] Rahaman, M.N. *Ceramic processing and sintering*, 2<sup>nd</sup> ed., Marcel dekker inc, New York, 2000.
- [36] “Sintering of a powder compact” [online]. Available from:  
[http://www.sv.vt.edu/classes/MSE2034\\_NoteBook/MSE2034\\_kriz\\_NoteBook/diffusion/apps/sinter.html](http://www.sv.vt.edu/classes/MSE2034_NoteBook/MSE2034_kriz_NoteBook/diffusion/apps/sinter.html) [2011, April 18]
- [37] Smart, L.E., Moore, E.A. *Solid state chemistry: An introduction*, 3<sup>rd</sup> ed., CRC Press, USA, 2005.
- [38] Dann, S.E. *Reactions and characterization of solids*, Royal Society of Chemistry, UK, 2000.
- [39] Wagner, C. In: *Proc. Int. Comm. Electrochem, Thermodyn. Kinetics, (CITCE)* vol. 7, Butterworth, London (1957), p. 361.

- [40] Wagner, C. Equations for transport in solid oxides and sulfides of transition metals *Solid State Chemistry* 10 (1975) 3 – 16.
- [41] Taheri, Z. et al. Oxygen permeation and oxidative coupling of methane in membrane reactor: A new facile synthesis method for selective perovskite catalyst. *J. Mol. Catal. A: Chem.* 286 (2008): 79–86.
- [42] Yin, Q. and Lin, Y. S. Effect of dopant addition on oxygen sorption properties of La-Sr-Co-Fe-O perovskite type oxide *Adsorption* 12 (2006) 329–338.
- [43] Tuller, H.L. Mixed conduction in nonstoichiometric oxides, in *Nonstoichiometric Oxides*, O.T. Sorensen, Editor. 1981, Academic Press: New York. p. 271-355.
- [44] Wang, Q.B., Yuan, Y., Han, M. and Zhu, P. Synthesis and characterization of  $\text{Ba}_{0.5}\text{Sr}_{0.5}\text{Co}_{0.8}\text{Fe}_{0.2}\text{O}_{3-\sigma}$  *Rare Metals* 28 (2009) 39 – 42.
- [45] Ge, L. et al. Properties and performance of A-site deficient  $(\text{Ba}_{0.5}\text{Sr}_{0.5})_{1-x}\text{Co}_{0.8}\text{Fe}_{0.2}\text{O}_{3-\delta}$  for oxygen permeating membrane *J. Membr.Sci.* 306 (2007) 318 – 328.
- [46] Lu, H., Cong, Y. and Yang, W.S. Oxygen permeability and stability of  $\text{Ba}_{0.5}\text{Sr}_{0.5}\text{Co}_{0.8}\text{Fe}_{0.2}\text{O}_{3-\delta}$  as an oxygen-permeable membrane at high pressures *Solid State Ionics* 177 (2006) 595 – 600.

## **APPENDICES**

## **APPENDIX A**

### The calculations for synthesis

The molecular weights of starting materials

Chemicals	Molecular weight	Metal	Molecular weight of metal
BaCO <sub>3</sub>	197.37	Ba	137.3
SrCO <sub>3</sub>	147.63	Sr	87.62
CoO	74.93	Co	58.93
Co <sub>3</sub> O <sub>4</sub> , powder	240.80	Co	58.93
Fe <sub>2</sub> O <sub>3</sub>	159.68	Fe	55.85
Nb <sub>2</sub> O <sub>5</sub>	265.81	Nb	92.91
La(NO <sub>3</sub> ) <sub>3</sub> ·6H <sub>2</sub> O	433.02	La	138.91
Sr(NO <sub>3</sub> ) <sub>2</sub>	211.63	Sr	87.62
Co(NO <sub>3</sub> ) <sub>2</sub> ·6H <sub>2</sub> O	291.03	Co	58.93
Fe(NO <sub>3</sub> ) <sub>3</sub> ·9H <sub>2</sub> O	404.00	Fe	55.85
Ni(NO <sub>3</sub> ) <sub>2</sub> ·6H <sub>2</sub> O	290.81	Ni	58.69
Citric acid	192.13	O	16.00

#### 1. Membrane materials by solid state method

Example Preparation of 1 g Ba<sub>0.5</sub>Sr<sub>0.5</sub>Co<sub>0.8</sub>Fe<sub>0.8</sub>O<sub>3</sub> (BSCF5582)

Molecular weight of BSCF5582 = 218.77 g/mol

$$\begin{aligned} \text{BSCF5582} \quad 218.77 \text{ g} &= 1 \text{ mol} \\ \text{BSCF5582} \quad 1 \text{ g} &= 1 \text{ g}/218.77 \text{ g} \\ &= 4.5709 \times 10^{-3} \text{ mol} \end{aligned}$$

Calculation of BaCO<sub>3</sub>

$$\begin{aligned} \text{BSCF5582} \quad 1 \text{ mol} &= \text{Ba } 0.5 \text{ mol} \\ \text{BSCF5582} \quad 4.5709 \times 10^{-3} \text{ mol} &= 0.5 \times 4.5709 \times 10^{-3} \text{ mol} \\ &= 2.2855 \times 10^{-3} \text{ mol} \\ \text{BaCO}_3 \quad 1 \text{ mol} &= 197.37 \text{ g} \\ \text{BaCO}_3 \quad 2.2855 \times 10^{-3} \text{ mol} &= 197.37 \times 2.2855 \times 10^{-3} \text{ g} \\ \text{Therefore, weighing BaCO}_3 &= 0.4511 \text{ g} \end{aligned}$$

Calculation of SrCO<sub>3</sub>

$$\begin{aligned} \text{BSCF5582} \quad 1 \text{ mol} &= \text{Sr } 0.5 \text{ mol} \\ \text{BSCF5582} \quad 4.5709 \times 10^{-3} \text{ mol} &= 0.5 \times 4.5709 \times 10^{-3} \text{ mol} \\ &= 2.2855 \times 10^{-3} \text{ mol} \\ \text{SrCO}_3 \quad 1 \text{ mol} &= 147.63 \text{ g} \end{aligned}$$



$$\begin{aligned} \text{SrCO}_3 \quad 2.2855 \times 10^{-3} \text{ mol} &= 147.63 \times 2.2855 \times 10^{-3} \text{ g} \\ \text{Therefore, weighing SrCO}_3 &= 0.3374 \text{ g} \end{aligned}$$

Calculation of  $\text{Co}_3\text{O}_4$

$$\begin{aligned} \text{BSCF5582} \quad 1 \text{ mol} &= \text{Co } 0.8 \text{ mol} \\ \text{BSCF5582} \quad 4.5709 \times 10^{-3} \text{ mol} &= 0.8 \times 4.5709 \times 10^{-3} \text{ mol} \\ &= 3.6567 \times 10^{-3} \text{ mol} \\ \text{Co}_3\text{O}_4 \quad 1 \text{ mol} &= 240.80 \text{ g} \\ \text{Co}_3\text{O}_4 \quad 2.2855 \times 10^{-3} \text{ mol} &= 240.80 \times 2.2855 \times 10^{-3} \text{ g} \\ \text{Therefore, weighing Co}_3\text{O}_4 &= 0.3374 \text{ g} \end{aligned}$$

Calculation of  $\text{Fe}_2\text{O}_3$

$$\begin{aligned} \text{BSCF5582} \quad 1 \text{ mol} &= \text{Fe } 0.2 \text{ mol} \\ \text{BSCF5582} \quad 4.5709 \times 10^{-3} \text{ mol} &= 0.8 \times 4.5709 \times 10^{-3} \text{ mol} \\ &= 9.1419 \times 10^{-4} \text{ mol} \\ \text{Fe}_2\text{O}_3 \quad 1 \text{ mol} &= 159.68 \text{ g} \\ \text{Fe}_2\text{O}_3 \quad 9.1419 \times 10^{-4} \text{ mol} &= 159.68 \times 9.1419 \times 10^{-4} \text{ g} \\ \text{Therefore, weighing Co}_3\text{O}_4 &= 0.0730 \text{ g} \end{aligned}$$

## 2. Catalysts by modified citrate method

Example Preparation of 1 g  $\text{La}_{0.1}\text{Sr}_{0.9}\text{Co}_{0.9}\text{Fe}_{0.1}\text{O}_3$  (LSCF1991)

Molecular weight of LSCF1991 = 199.37 g/mol

$$\begin{aligned} \text{LSCF1991} \quad 199.37 \text{ g} &= 1 \text{ mol} \\ \text{LSCF1991} \quad 1 \text{ g} &= 1 \text{ g}/199.37 \text{ g} \\ &= 5.0158 \times 10^{-3} \text{ mol} \end{aligned}$$

Calculation of  $\text{La}(\text{NO}_3)_3 \cdot 6\text{H}_2\text{O}$

$$\begin{aligned} \text{LSCF1991} \quad 1 \text{ mol} &= \text{La } 0.1 \text{ mol} \\ \text{LSCF1991} \quad 5.0158 \times 10^{-3} \text{ mol} &= 0.1 \times 5.0158 \times 10^{-3} \text{ mol} \\ &= 5.0158 \times 10^{-4} \text{ mol} \\ \text{La}(\text{NO}_3)_3 \cdot 6\text{H}_2\text{O} \quad 1 \text{ mol} &= 433.02 \text{ g} \end{aligned}$$

$$\begin{aligned} \text{La(NO}_3)_3 \cdot 6\text{H}_2\text{O} \quad 5.0158 \times 10^{-4} \text{ mol} &= 433.02 \times 5.0158 \times 10^{-4} \text{ g} \\ \text{Therefore, weighing La(NO}_3)_3 \cdot 6\text{H}_2\text{O} &= 0.2172 \text{ g} \end{aligned}$$

#### Calculation of Sr(NO<sub>3</sub>)<sub>2</sub>

$$\begin{aligned} \text{LSCF1991} \quad 1 \text{ mol} &= \text{Sr } 0.9 \text{ mol} \\ \text{LSCF1991} \quad 5.0158 \times 10^{-3} \text{ mol} &= 0.9 \times 5.0158 \times 10^{-3} \text{ mol} \\ &= 4.5140 \times 10^{-3} \text{ mol} \\ \text{Sr(NO}_3)_2 \quad 1 \text{ mol} &= 211.63 \text{ g} \\ \text{Sr(NO}_3)_2 \quad 4.5140 \times 10^{-3} \text{ mol} &= 211.63 \times 4.5140 \times 10^{-3} \text{ g} \\ \text{Therefore, weighing Sr(NO}_3)_2 &= 0.9553 \text{ g} \end{aligned}$$

#### Calculation of Co(NO<sub>3</sub>)<sub>2</sub>·6H<sub>2</sub>O

$$\begin{aligned} \text{LSCF1991} \quad 1 \text{ mol} &= \text{Co } 0.9 \text{ mol} \\ \text{LSCF1991} \quad 5.0158 \times 10^{-3} \text{ mol} &= 0.9 \times 5.0158 \times 10^{-3} \text{ mol} \\ &= 4.5140 \times 10^{-3} \text{ mol} \\ \text{Co(NO}_3)_2 \cdot 6\text{H}_2\text{O} \quad 1 \text{ mol} &= 291.03 \text{ g} \\ \text{Co(NO}_3)_2 \cdot 6\text{H}_2\text{O} \quad 4.5140 \times 10^{-3} \text{ mol} &= 291.03 \times 4.5140 \times 10^{-3} \text{ g} \\ \text{Therefore, weighing Co(NO}_3)_2 \cdot 6\text{H}_2\text{O} &= 1.3138 \text{ g} \end{aligned}$$

#### Calculation of Fe(NO<sub>3</sub>)<sub>3</sub>·9H<sub>2</sub>O

$$\begin{aligned} \text{LSCF1991} \quad 1 \text{ mol} &= \text{Fe } 0.1 \text{ mol} \\ \text{LSCF1991} \quad 5.0158 \times 10^{-3} \text{ mol} &= 0.1 \times 5.0158 \times 10^{-3} \text{ mol} \\ &= 5.0158 \times 10^{-4} \text{ mol} \\ \text{Fe(NO}_3)_3 \cdot 9\text{H}_2\text{O} \quad 1 \text{ mol} &= 404.00 \text{ g} \\ \text{Fe(NO}_3)_3 \cdot 9\text{H}_2\text{O} \quad 5.0158 \times 10^{-4} \text{ mol} &= 404.00 \times 5.0158 \times 10^{-4} \text{ g} \\ \text{Therefore, weighing Fe(NO}_3)_3 \cdot 9\text{H}_2\text{O} &= 0.1013 \text{ g} \end{aligned}$$

#### Citric acid

General formula of perovskite is ABO<sub>3</sub>, calculation base on  $5.0158 \times 10^{-3}$  mole LSCF1991

To form the complex, moles of metal : moles of citric acid = 1:1

$$\begin{aligned}
 &\text{In La(NO}_3)_3 \cdot 6\text{H}_2\text{O, the amount of metal [NO}_3\text{]} = 3 \text{ mole} \\
 &\text{For } 2.8880 \times 10^{-3} \text{ mole of La(NO}_3)_3 \cdot 6\text{H}_2\text{O} \quad \frac{3 \text{ mole} \times 5.0158 \times 10^{-3} \text{ mole}}{1 \text{ mole}} \\
 &= 1.5047 \times 10^{-2} \text{ mole}
 \end{aligned}$$

$$\begin{aligned}
 &\text{In Sr(NO}_3)_2, \text{ the amount of metal [NO}_3\text{]} = 2 \text{ mole} \\
 &\text{For } 2.8880 \times 10^{-3} \text{ mole of Sr(NO}_3)_2 \quad \frac{2 \text{ mole} \times 5.0158 \times 10^{-3} \text{ mole}}{1 \text{ mole}} \\
 &= 1.0032 \times 10^{-2} \text{ mole}
 \end{aligned}$$

$$\begin{aligned}
 &\text{In Co(NO}_3)_2 \cdot 6\text{H}_2\text{O, the amount of metal [NO}_3\text{]} = 2 \text{ mole} \\
 &\text{For } 2.5992 \times 10^{-3} \text{ mole of Co(NO}_3)_2 \cdot 6\text{H}_2\text{O} \quad \frac{2 \text{ mole} \times 5.0158 \times 10^{-3} \text{ mole}}{1 \text{ mole}} \\
 &= 1.0032 \times 10^{-2} \text{ mole}
 \end{aligned}$$

$$\begin{aligned}
 &\text{In Fe(NO}_3)_3 \cdot 9\text{H}_2\text{O, the amount of metal [NO}_3\text{]} = 3 \text{ mole} \\
 &\text{For } 2.8880 \times 10^{-4} \text{ mole of Fe(NO}_3)_3 \cdot 9\text{H}_2\text{O} \quad \frac{3 \text{ mole} \times 5.0158 \times 10^{-3} \text{ mole}}{1 \text{ mole}} \\
 &= 1.5047 \times 10^{-2} \text{ mole}
 \end{aligned}$$

$$\begin{aligned}
 \text{Total amount of [NO}_3\text{]} &= (1.5047 + 1.0032 + 1.0032 + 1.5047) \times 10^{-2} \text{ mole} \\
 &= 0.0502 \text{ mole}
 \end{aligned}$$

$$\begin{aligned}
 \text{Weight of citric acid} &= n \times \text{MW} \\
 &= 0.0502 \times 192.13 = 9.6368 \text{ g}
 \end{aligned}$$

## **APPENDIX B**

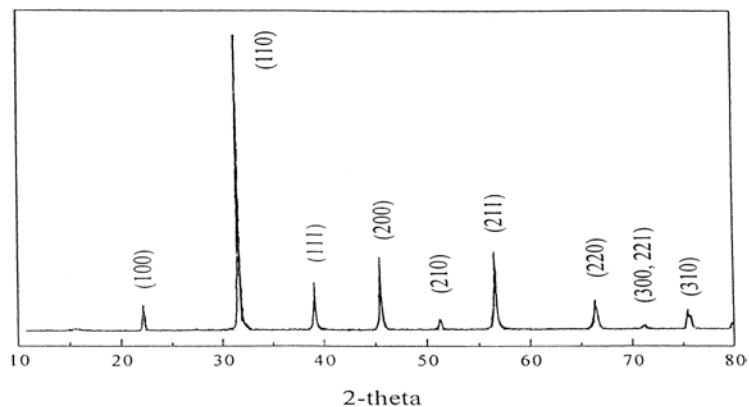


**Figure 1** XRD pattern of BSCF reported by Shao and co-workers [9].

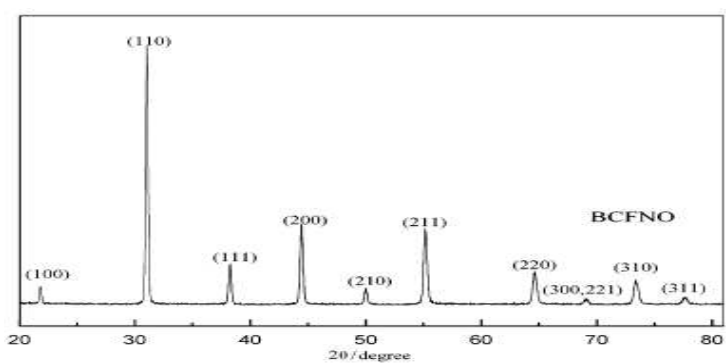


**Figure 2** XRD pattern of BCFNO reported by Zhang and co-workers [19].

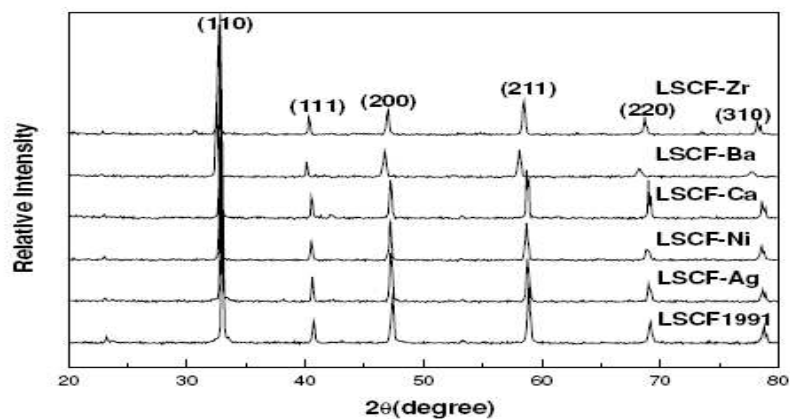


**Figure 3** XRD patterns of LSCF1991 reported by Yin and co-workers [42].

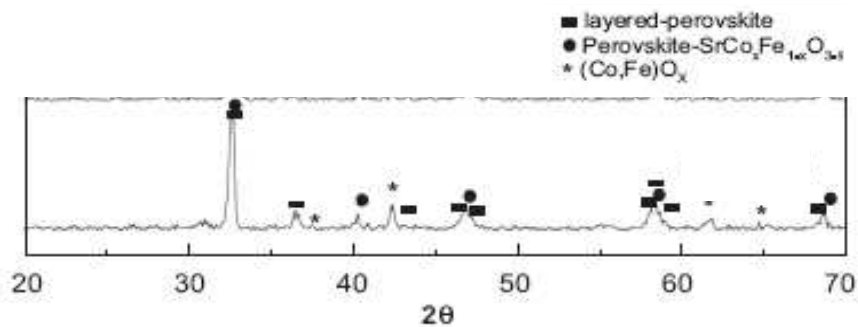


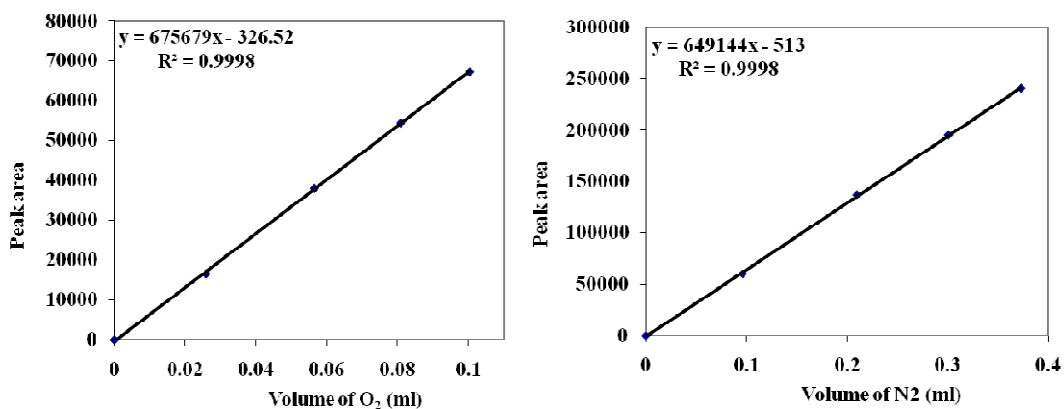
**Figure 4** XRD pattern of SCF reported by Yin and co-workers [24].

## **APPENDIX C**

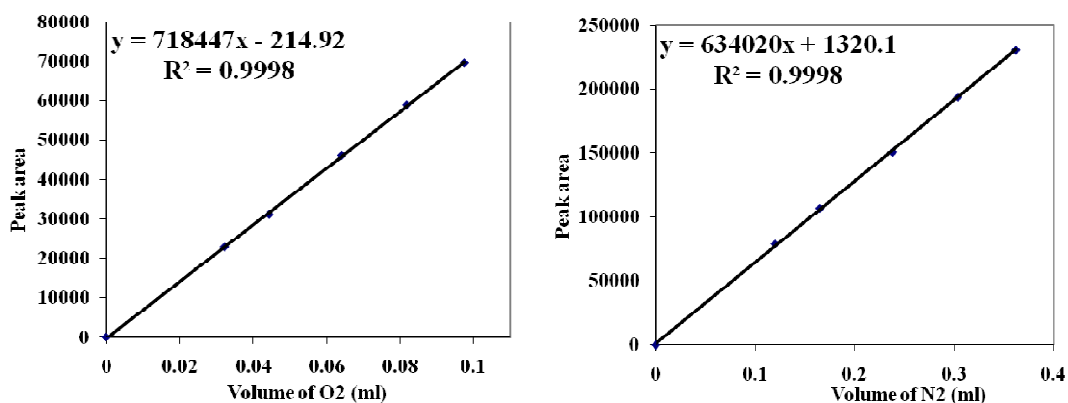
### The calibration curves of oxygen and nitrogen

Used for membrane reactor analysed by gas chromatography (HP 6820)

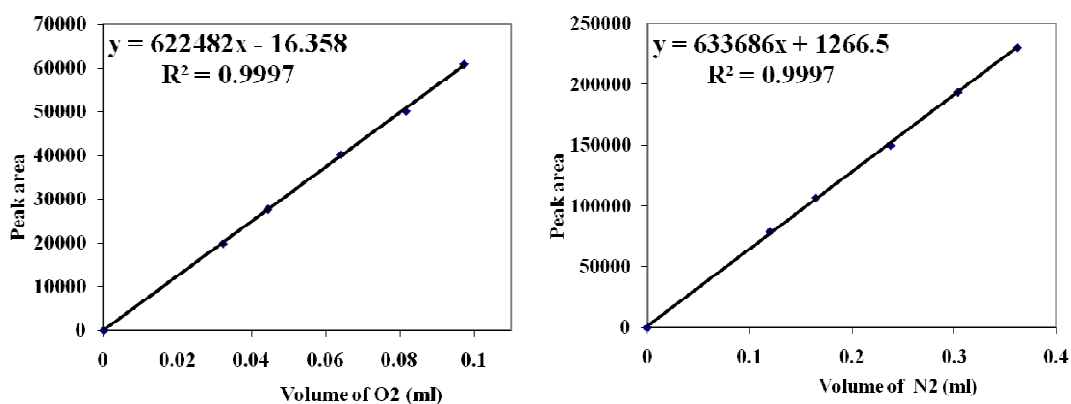
August 2010



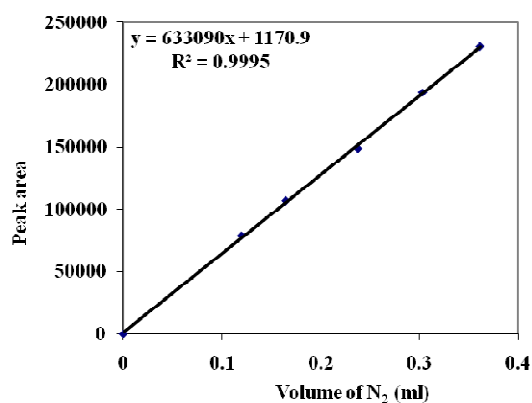
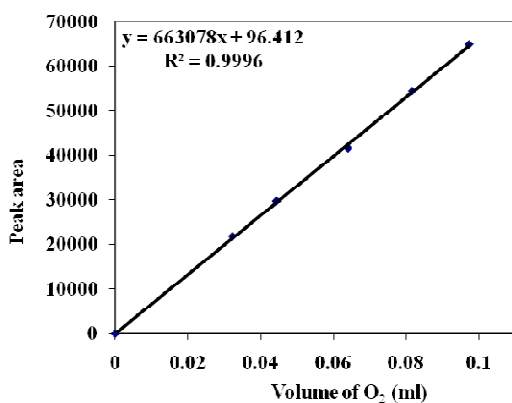
September 2010



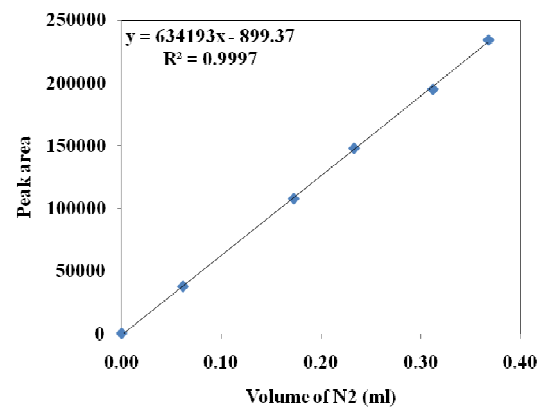
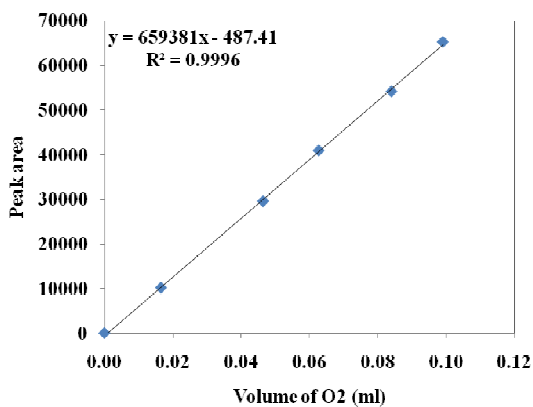
October 2010



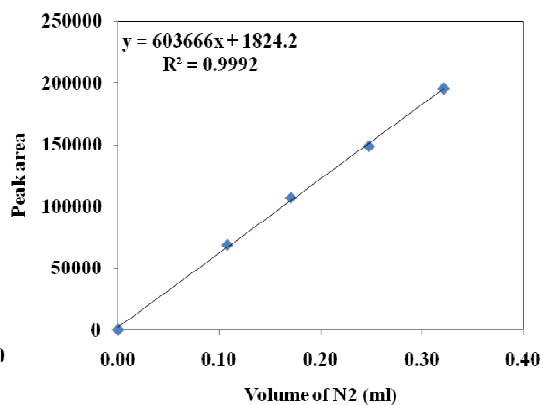
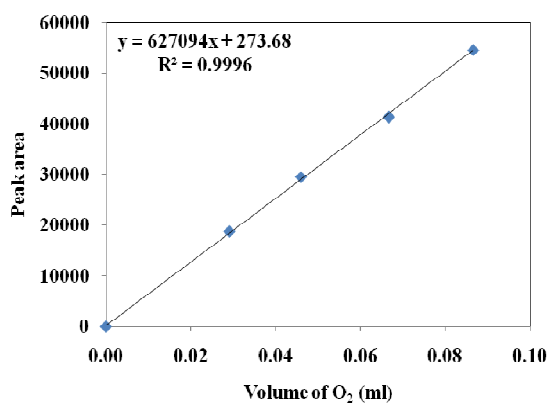
## November 2010



## December 2010

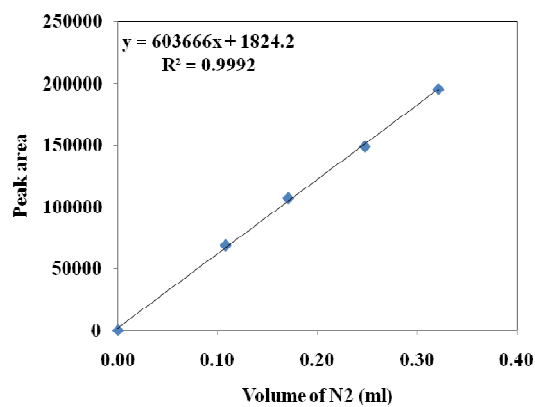
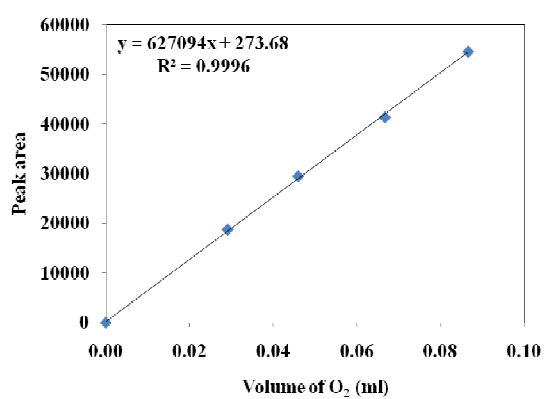


## January 2011

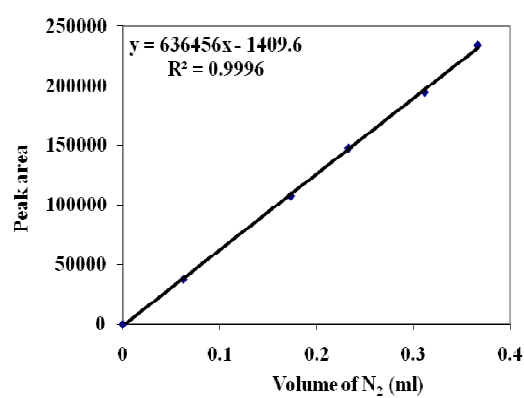
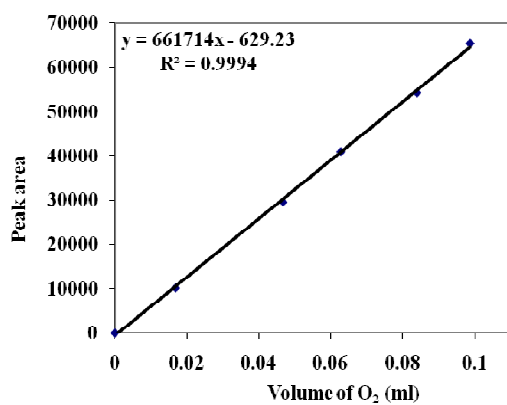




## February 2011



## March 2011



## **APPENDIX D**

### Calculation of oxygen permeation flux

Example The BSCF membrane coated by SCF on the He side was tested for the oxygen permeation on August 2010. At 1000°C, the obtained peak areas of oxygen and nitrogen are 40119  $\mu\text{V}\cdot\text{s}$  and 723.37  $\mu\text{V}\cdot\text{s}$ , respectively (measured by GC with sample loop of 1 ml). The flow rate of gas on sweep side is 53.58 ml/min and the membrane geometric surface area of the sweep side is 1.32  $\text{cm}^2$ . According to the linear equations from the calibration curve of oxygen and nitrogen for January 2011, the concentration of oxygen and nitrogen were calculated below.

Linear equation of oxygen;  $y = 659381x - 487.41$

$$y = 40119 \mu\text{V}\cdot\text{s}, \text{ so } x = 0.0616 \text{ ml}$$

Because of the volume of the sample loop is 1 ml, therefore the concentration of oxygen is 0.0616 ml/ml.

Linear equation of nitrogen;  $y = 634193x - 899.37$

$$y = 723.37 \mu\text{V}\cdot\text{s}, \text{ so } x = 0.0026 \text{ ml}$$

Because of the volume of the sample loop is 1 ml, therefore the concentration of nitrogen is 0.0026 ml/ml.

The oxygen permeation flux,  $J_{\text{O}_2}$ , can calculate by equation below.

$$\begin{aligned} J_{\text{O}_2} &= \left[ C_{\text{O}_2} - C_{\text{N}_2} \times \frac{0.21}{0.79} \times \left( \frac{28}{32} \right)^{\frac{1}{2}} \right] \times \frac{F}{S} \\ &= \left[ 0.0616 - 0.0026 \times \frac{0.21}{0.79} \times \left( \frac{28}{32} \right)^{\frac{1}{2}} \right] \times \frac{53.58 \text{ ml/min}}{1.32 \text{ cm}^2} \\ &= 2.47 \text{ ml/min}\cdot\text{cm}^2 \end{aligned}$$

Therefore the oxygen permeation flux of BSCF membrane coated by SCF on He side is 2.47  $\text{ml/min}\cdot\text{cm}^2$  at the temperature of 1000°C.

## VITAE

Mister Soontorn Suvokhiaw was born on September 22, 1985 in Roi Et, Thailand. He received Bachelor's Degree of Science in Chemistry from Khon Kaen University in 2008. Since then, he attended the Master's Degree Department of Chemistry at Faculty of Science, Chulalongkorn University and finished his study in 2011.

### **Presentation**

5 – 7 January 2011

Poster presentation “Improving the oxygen permeability of barium or lanthanum-based perovskite membranes by surface-coating with catalysts” The Pure and Applied Chemistry International Conference (PACCON2011), Miracle grand hotel, Bangkok.

His present address is 57 Naloeng, Selaphum, Roi Et, 45120, Thailand. Tel 084-5155654, E-mail: s\_suntornsc@hotmail.com.